On the Performance of Connectivity of Cellular Based IoT Network

by

Syeda Puspita Mouri

B.Sc. Hons., Military Institute of Science & Technology, Bangladesh, 2016

A THESIS SUBMITTED IN PARTIAL FULFILLMENT OF
THE REQUIREMENTS FOR THE DEGREE OF

MASTER OF APPLIED SCIENCE

in

THE COLLEGE OF GRADUATE STUDIES

(Electrical Engineering)

THE UNIVERSITY OF BRITISH COLUMBIA

(Okanagan)

May 2019

The following individuals certify that they have read, and recommend to the College of Graduate Studies for acceptance, a thesis/dissertation entitled:

On the Performance of Connectivity of Cellular Based IoT Network

submitted by Syeda Puspita Mouri in partial fulfilment of the requirements of the degree of Master of Applied Science

Dr. Md. Jahangir Hossain, School of Engineering
Supervisor

Dr. Stephen O'Leary, School of Engineering
Supervisory Committee Member

Dr. Anas Chaaban, School of Engineering
Supervisory Committee Member

Dr. Keekyoung Kim, School of Engineering
University Examiner

Abstract

Due to the manifold connected devices future cellular based Internet of Things (IoT) networks require significant attention. Random point process (PP) based networks models are now widely accepted models for designing cellular based IoT networks because of theirs analytical tractability. This thesis focuses on analyzing the performance of cellular networks for massive connectivity of IoT devices using stochastic geometry.

In cellular based IoT network, one of the key challenges resides in establishing connection between the devices and the base stations (BSs). An IoT device performs random access channel (RACH) procedure when it needs to establish connection with its intended BS. This thesis specifically focuses on the study of success of RACH access procedure for different BSs' distribution.

In particular, we propose a novel generalized approach to calculate connection failure probability of IoT devices in RACH phase of uplink (UL) transmission. The proposed approach uses a calculation of the devices' association probability rather than an approximation of the Voronoi tessellation's cell area distribution. There are some limitations of using Voronoi tessellation based approach. This approach can only be used when the BSs are distributed according to Poisson point process (PPP). The merit of the proposed approach, besides its exact analysis, is that it can be applied for general scenarios of BSs' distributions. To adopt this approach, we derive the void probability for different Poisson cluster processes (PCP), in particular, Matérn cluster process (MCP) and Thomas cluster process (TCP), which is defined as the probability of having no children point of PCP in a given distance.

First, we use our proposed mathematical approach to single-tier network.

Next, we extend our mathematical framework in multi-tier cellular based IoT network. For both types of networks, we investigate the performance metrics using PPP and PCP distributions for BSs' deployment. We validate our approach with the numerical simulations via MATLAB. We vary different network parameters to see the effect in failure probability which can help network designers to set values of various design parameters. Numerical results demonstrate that our mathematical framework is highly accurate and adaptable for general scenarios.

Lay Summary

Internet of Things (IoT) is a digital revolution, which refers to a massive number of connected devices. Due to manifold devices, IoT networks are being challenged by several connectivity issues. One of the most attractive solutions to these issues is cellular network architecture because of its adaptability and availability. Traditional hexagonal cellular networks are less practical, and this type of network architecture can not be used for a massive number of devices. Hence, introducing randomness in the deployment of nodes, i.e., transceiver and IoT devices, is more practical solution to this problem. Again, conventional communication theory, somewhat, falls short to portray the random nature of interference. Stochastic geometry is an efficient tool to capture the randomness of the interference. Our work exploits stochastic geometry to develop a novel mathematical approach to measure the performance metrics for different types of random deployment of nodes.

Preface

This thesis is based on the research work conducted in the School of Engineering at The University of British Columbia's Okanagan campus under the supervision of Prof. Md. Jahangir Hossain.

I like to specify that the research idea, analytical evaluations, and numerical simulations related to the publication are the results of my own work. I am the principle investigator of the research works documented in the thesis. Along with Prof. Hossain, Dr. Mahdi Ben Ghorbel, who was working as a Post Doctoral Fellow with Dr. Hossain, also helped to prepare the manuscript by checking the validity of analytical and numerical results, and proofreading the presentations.

Table of Contents

List of Tables

List of Figures

Acronyms	Definitions
AES	Advanced Encryption Standard
BS	Base Station
DL	Downlink
IDC	International Data Corporation
IoT	Internet of Things
LTE	Long Term Evolution
MAC	Media Access Control
MBS	Macro Base Station
MCP	Matern Cluster Process
MGF	Moment Generating Function
PCP	Poisson Cluster Process
PGF	Probability Generating Function
PP	Point Process
PPP	Poisson Point Process
PRACH	Physical Random Access Channel
RACH	Random Access Channel
SBS	Small Base Station
SINR	Signal-to-Interference-Plus-Noise-Ratio
SSL	Secure Sockets Layer
TCP	Thomas Cluster Process
TSL	Transport Layer Security
UL	Uplink

Acknowledgements

I am deeply grateful to my supervisor Prof. Jahangir Hossain for his enthusiasm, guidance, advice, encouragement, and support. He granted me a great flexibility and freedom in my research work. I am privileged to have the opportunity to conduct my graduate study under his supervision.

I would like to express my thanks to Prof. Keekyoung Kim to serve as my external examiner. I would also like to thank Prof. Stephen O'Leary and Prof. Anas Chaaban for serving on the committee. I really appreciate their valuable time and constructive comments on my thesis.

I owe many people for their generosity and support during my MASc study at The University of British Columbia. I would like thank Dr. Mahdi Ben Ghorbel, former post-doctoral fellow working with Dr. Hossain, for his guidance. I would like to thank my dear colleagues Dr. Zoheb Hassan, Dr. Hassan M. Navazi, and Mohammed Alabiad for sharing their academic experiences and constructive viewpoints generously with me during our discussions.

I would like to thank my parents and parents-in-law for their patience, understanding, and blessings all these years. I want to specially mention my father, for instilling me with a strong passion for learning, and doing anything and everything to put me on a path towards success. I am also grateful to my husband Rasel for his unceasing encouragement, support, and attention throughout this venture. All my achievements would not have been possible without constant support from my family.

Finally, I take this opportunity to express gratitude to all of the faculty and staff members of School of Engineering for their help and support. I also place on record, my sense of gratitude to one and all, who directly or indirectly, have lent their hand in this venture.

Chapter 1

Introduction

1.1 Background and Motivation

Twenty years ago, when people used to get stuck in traffic, they had nothing to do but to wait. Now people can check the route with the lowest traffic before they start and avoid inconvenience. It can be predicted that after twenty years, cars will have a calendar schedule, and they will decide when to start and what route to take. This is an example of the digital revolution. This digital revolution, which impacts all aspects of life, is called Internet of Things (IoT) [1, 2].

IoT is emerging as the next stage of the information revolution [3]. It has the potential to transform the world as it is capable of revolutionizing our lives through manifold applications, e.g., in smart homes, smart cities, security, tracking, vehicular connectivity, environment, and e-health [4–6]. The main concept of IoT is to inter-connect massive number of devices. IoT can be considered as an association or group of devices that are connected to collect and share data [4]. Hence, this technology is large scale by nature [5, 7].

The concept of IoT began to emerge in 1999 [8, 9], and according to a recent forecast, International Data Corporation (IDC) expects 212 billion connected "things" globally by the end of 2020 [6]. A report from ABI Research predicts that 75% of the growth in wireless connections between today and the end of the decade will come from non-hub devices, that is, sensor nodes and accessories [10–12]. Apart from mainstream mobile devices, billions of IoT devices or connections will be added by the end of 2021 [11, 13, 14]. Table 1.1 depicts the growth of number of connected devices and connected devices per person in IoT network since 2003 [13]. The

vast revolution in the number of connected devices mainly took place in the year of 2008 and 2009, and at that point of time more "things" started to get connected than people [13]. A graphical representation of Table 1.1 is shown in Fig. 1.1. This figure shows the trend of increment on number of connected devices over the past years.

Table 1.1: Increasing Trend of IoT Devices

Year	World population	Connected devices	Connected device per person
2003	6.3 billion	500 million	0.08
2010	6.8 billion	12.5 billion	1.84
2015	7.2 billion	25 billion	3.47

IoT is expected to bring revolutionary change in every sphere of lives [15, 16]. Smart cities, smart home, automation in agriculture, transportation, health care, and others are the most near future result of IoT. In future, it can be possible to predict the natural disasters and take necessary measures with the combination of sensors and automations. To confirm the deployment of large number of sensors to facilitate the emergence of IoT it is expected that the average price of sensors would fall from 50 cent to 38 cent by 2020 [17]. Water scarcity monitoring, managing energy consumption at home, and even monitoring health parameters automatically is possible now [15, 17]. Philips has developed a device that will send a pop up message when it is time to take medicines to confirm an assistance to ill people [17]. This kind of change in each sector of life shows how rapidly IoT is making its place.

1.1.1 Connectivity Challenges in Internet of Things

Modern era of communication is looking for the interconnection among the enormous number of devices. Hence, IoT is a massive-scale technology by nature. High volumes of traffic are to be accommodated in the network. To accommodate this huge traffic IoT is facing several connectivity issues which are discussed below [16, 18].

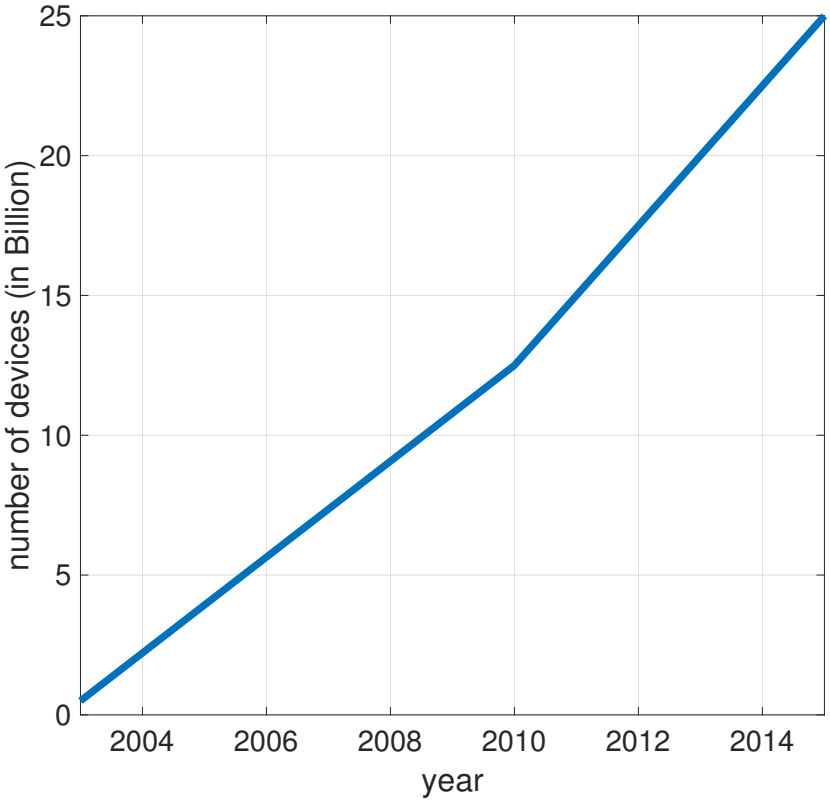

Figure 1.1: Trend of increasing number of connected devices.

1.1.1.1 Reliable signalling

When we think about servers and connected devices, a concern is about the data, that the devices are generating and absorbing, which is called data stream. Sometimes the devices need to talk with the server, sometimes the server needs to talk with the devices, and sometimes the devices need to talk with each other. In either case, we may have issues with connectivity drop off. We need to make sure the stream of data travel to their destination. So, here we need reliable two way signalling (bi-directional signalling) [19]. Hence, one of the main and challenging requirements for the success of IoT is the availability of uninterrupted, reliable as well as bi-directional signalling which should be enough for collecting as well as routing all data between two or more than two devices.

1.1.1.2 Security

Devices face security challenges while connecting to each other or to base station (BS) [20]. Below are the few main aspects of security challenges faced in the IoT technology.

1.1.1.2.1 Encryption: There will be the need for reliable and appropriate end to end encryption for all the devices as well as their respective servers. Transport layer security (TLS) or secure sockets layer (SSL) can not be applied here because these are used for point to point encryption, not end to end encryption. In IoT deployment data has to go through number of different points along the chain or path, and so encryption is needed to be confirmed throughout the data life cycle. Advanced encryption standard (AES) can be a good choice of end to end encryption.

1.1.1.2.2 Authorization: When we send a data stream or receive a data stream, we need to make sure that the device has authorization to receive or send that particular data stream. This is due to the cause that streaming of data between servers and devices is one of the most crucial aspects of the IoT technology [21].

1.1.1.2.3 Open ports: Open ports can be a cause of much trouble for all devices if they are left unused. Open ports may prove vulnerable in contact with the internet. This is where the need for bi-directional communication arises since we will certainly not want to expose any open ports to the internet.

1.1.1.3 Power consumption

With millions of different IoT devices sending as well as receiving data, it takes a toll on the CPU consumption and power. With all this complex communication taking place 24×7, what we will need, is a network that does not drain the battery of our device and must consume less power as well [22].

1.1.1.4 Detection of presence

One of the main concerns of being connected over a common network is to be aware of when the IoT device will be dropping off the network and go offline without any prior notice. Also, there is no way to know when the device will get connected back to the network and go online. It is needed to monitor the presence of the devices in the network. The network designer needs to know when the device went offline, when it came back to online and the history when the device was offline.

1.1.1.5 Bandwidth

Bandwidth limitation is going to be one of the major challenges in massive IoT network. As IoT deals with massive number of devices, transferring data among devices and with the servers causes network jamming. A large scale network is needed to handle the massive amount of data. It is needed to create a network where devices can seamlessly transfer data as smoothly as possible.

Overall, to ensure connectivity of massive number of IoT devices, there will be a number of challenges, mainly scalability, heterogeneity, and context

awareness issues that are unique to IoT application scenarios. Table 1.2 summarizes the challenges on connectivity of IoT devices.

Table 1.2: Connectivity Challenges of IoT

Type	Feature
Reliable signalling	Need to make sure that data stream can travel from the start point to the desired end point.
Security	Proper encryption and authorization have to be confirmed, and open ports should be taken care of.
Power consumption	Need to build up a network that consumes less CPU power.
Detection of presence	Need to know when a device goes offline, and when it comes back to online.
Bandwidth	Need to build a network which can deal with massive IoT traffic.

1.1.2 Solution to Connectivity Challenges

In order to provide connectivity for IoT devices, research and development in designing various wireless network architectures have been making progress in recent years. The existing cellular networks are a natural and attractive solution to provide connectivity to IoT devices due to their worldwide-established footprint and the capillary market penetration [12], [23]. Random channel access is a preferred option due to the massive number of connected devices. However, cellular networks may have scalability problems to provide uplink connectivity to massive numbers of connected things and several studies report scalability issues in cellular networks for supporting massive uplink devices due to the random access based uplink scheduling, e.g., see [12, 24–26] and references there in.

One of the key challenges for IoT network is the deployment and ensuring connectivity of enormous number of devices in the network. Single-tier network, where the network only has one type of BSs, suffers from the connec-

tivity issues of large number of IoT devices [27]. One of the effective solutions of the connectivity issue is to use multi-tier topology where multiple types of BSs with dissimilar characteristics such as coverage areas, transmit powers, and etc. are deployed. Multi-tier cellular networks offer a fast, flexible and improved network expansion for the existing cellular architecture [27]. Even clustered single-tier networks are subjected to have higher connection failure probability than the multi-tier clustered networks. In a single-tier network if the BSs are clustered, some of the devices will be far from them which will result into low signal power and high interference power. These will eventually lead to high failure probability. Although multi-tier networks offer benefits, two main challenges appear while dealing with multi-tier networks as follows. First, we need to develop system models that capture the realistic heterogeneity in infrastructure, irregularity in the BS locations, and other key characteristics of multi-tier networks. Second, we need to develop corresponding analytical frameworks to study performance metrics like failure probability as a function of signal-to-interference-plus-noise-ratio (SINR), outage probability, delay, and etc.

Traditionally, cellular networks are modelled using hexagonal grid model having the BSs in the centre of the hexagonal cell. A realization of hexagonal grid model is shown in Fig. 1.2. This model has become questionable for current deployment scenarios of BSs [28, 29]. Point processes (PP) became popular to model cellular networks due to their practicality and analytical tractability using stochastic geometry tools [30, 31]. According to these models, BSs are placed in a random manner rather than the predetermined positions in hexagonal grid models. As a result, point processes present the advantage of modelling the current generation of cellular networks.

Mostly, Poisson point process (PPP) has been used to model wireless communication networks due to its analytical tractability. According to PPP, the BSs/devices are assumed to be spatially uniformly distributed. However, this assumption may not portrait all the cellular BSs' deployment scenarios. Therefore, researchers have considered Poisson cluster process (PCP). Clustering gives freedom to specify offspring points in different areas around the parent [32]. With PCP, the parent points are distributed

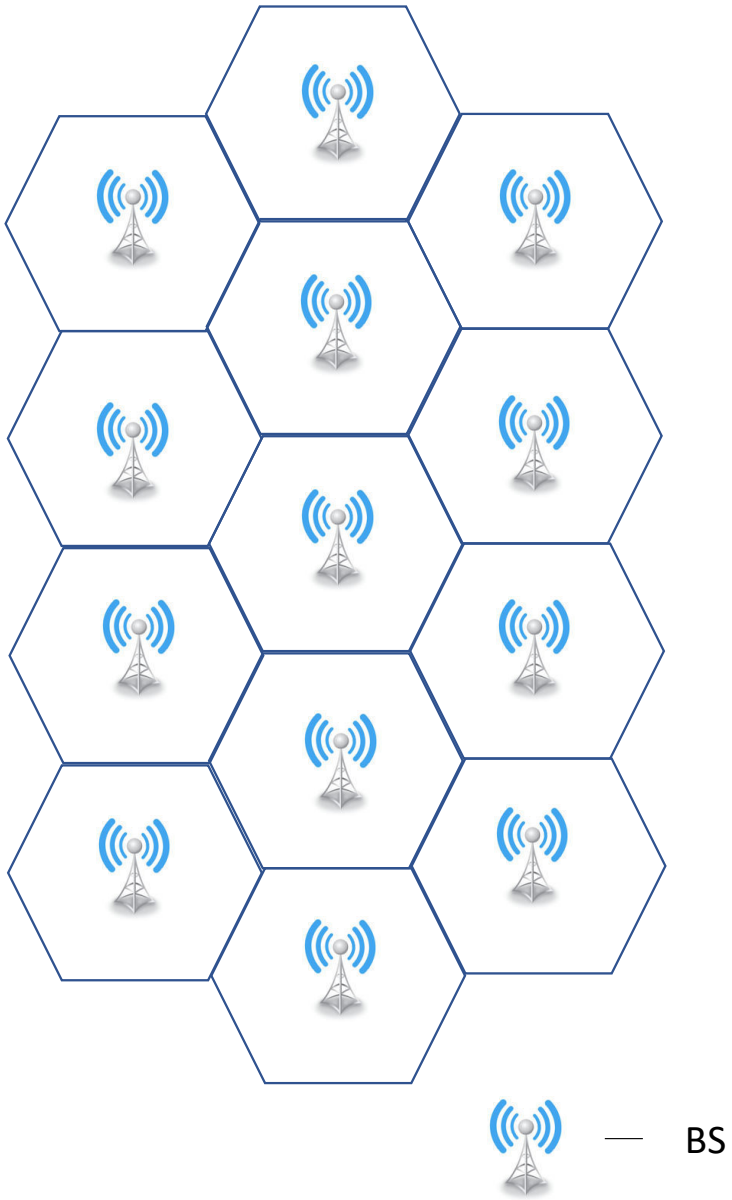

Figure 1.2: A realization of hexagonal grid cellular network model.

exponentially in the area and the offspring points are distributed around the parent points. In PCP, two of the widely used distributions are Matérn cluster process (MCP) and Thomas cluster process (TCP). In MCP, the offspring points are uniformly distributed in a disk of a certain radius around the parent points. In TCP, the offspring points follow normal distribution around the parent points. The challenge of using PCP is that the distribution of contact distances, which are the distances between the devices and their associated BSs, is difficult to obtain for certain devices' and BSs' distributions. A realization of PCP multi-tier network is shown in Fig. 1.3 where the macro base stations (MBSs) are deployed as the parent points of the PCP and small base stations (SBSs) are deployed as the children points of PCP.

An IoT device performs RACH procedure [25, 33] when it needs to establish connection with its intended BS. RACH is primarily used for initial network access in cellular network and after a successful RACH phase, data transmission between the device and BS takes place. Stochastic geometry combining with queuing theory and probability theory have been considered as one of the most efficient tools to model and analyze the stability and scalability characteristics of the connection request phase of massive IoT network [25, 34]. The importance of investigating the RACH access phase in IoT enabled network is that in this phase we need to consider numerous number of devices trying to connect with the same BS, which generates intra-cell interference. In the transmission phase, where only one device is connected to a BS, the only interference it needs to encounter is inter-cell interference which decreases the complexity of the mathematical model.

1.2 Literature Review

Recent research works have developed a spatio-temporal analytical model to study the scalability and stability of single-tier cellular systems and determine the IoT uplink traffic limits they can accommodate [12, 24–26]. The developed model accounts for traffic requirements and devices distributions as well as the mutual inter-cell and intra-cell interference using a combined

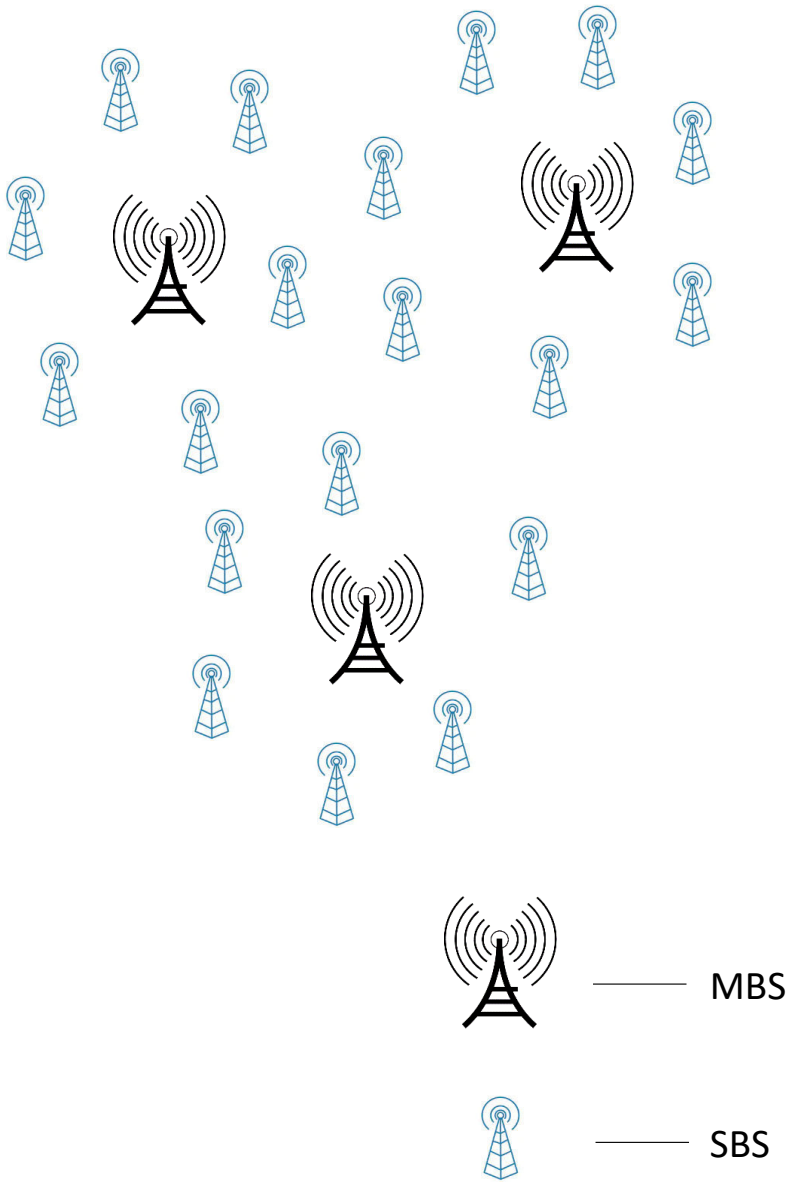

Figure 1.3: A realization of multi-tier (two-tier) PCP network.

stochastic geometry and queuing theory approach. In the above mentioned works, the authors focus on calculating failure probability for RACH access phase. In these works an approximation is used to calculate the number of devices associated to each BS. Considering that the BSs are distributed according to a PPP, the covered area by each BS is a Voronoi cell, whose area was approximated by using the Gamma distribution. As a result, the authors approximated the distribution of the devices associated per BS in order to calculate the Laplace transform of interference power. This approximation is applicable for PPP. Although PPP is analytically tractable, it may not be realistic for many BSs deployment scenarios as mentioned earlier.

A number of recent works have considered using PCP for analyzing cellular networks performance [35, 36]. Most of the recent works considered single-tier downlink (DL) transmission scenario. In [35, 36] authors considered multi-tier scenario for DL. In [37], authors studied the outage probability of UL transmission for multi-tier PPP network, considering only one MBS in their system model. Authors in [24, 25, 34] considered RACH phase of UL transmission scenario, with single-tier PPP network for IoT connectivity using the approximation of Voronoi tessellation for coverage area of a BS. Such an assumption simplifies the analysis, however, it is not a valid assumption for random access protocol on PCP multi-tier network with a massive number of devices. With PCP multi-tier networks, the main difficulty resides in finding the distributions of the interfering devices in cell and from other cells. Dealing with the scenario of multiple devices associated per channel per BS is even more challenging for MCP as devices/BS are not uniformly distributed.

Motivated by the above mentioned limitations of the existing works, in this work, we develop an innovative approach to analyze connection failure probability of RACH phase of UL single-tier and multi-tier cellular networks for massive connectivity of IoT devices. To demonstrate the adoptability and accuracy of this novel approach we consider the following cases for BSs' distribution while devices are PPP distributed in all of these the cases.

- BSs are distributed according to PPP in a single-tier network,
- BSs are distributed according to children points of PCP (MCP and TCP) in a single-tier network,
- BSs are distributed according to PPP in a multi-tier network,
- BSs are distributed according to parents and children points of PCP (MCP and TCP) in a multi-tier network,

1.3 Thesis Outline and Contributions

The thesis is arranged into five chapters. Chapter 1 presents background knowledge on the history and development of IoT enabled cellular network. In addition, this chapter provides a detailed literature review related to the rest of this thesis.

Chapter 2 presents the required technical background for the thesis. We first introduce different Point Processes, for instance, PPP, PCP. We emphasis on the usefulness of stochastic geometry on cellular network. We also discuss about characterizing the interference using stochastic geometry.

Chapter 3 provides highly accurate mathematical model to calculate failure probability for IoT enabled single-tier network. Here we consider 3 models for BSs' distribution. First, we consider the BSs are distributed according to children points of MCP. We derive the mathematical model for connection failure probability at each time slot in RACH access phase. Second, we consider BSs are distributed according to TCP and we use our novel mathematical approach in this system model to find the connection failure probability. Third, we consider BSs are distributed according to PPP and we implement our mathematical framework in this system model to find the connection failure probability. We also plot the connection failure probability using Voronoi-approximation for cell coverage area, which was used in [24]. By comparing our mathematical model with conventional Voronoi-approximation model, we conclude that our model is adaptable and accurate for both PPP and PCP distribution of BSs.

The motivation of Chapter 4 is to build a generalized mathematical model to analyze the performance of multi-tier IoT enabled cellular network. In this chapter, we investigate the connection failure probability for multi-tier IoT enabled cellular network. We consider PPP and PCP distribution for BSs' deployment in three different system models. For association of the devices to BSs we consider two schemes: (i) *distance threshold-based association*, and (ii) *power-based association*. Some interesting findings are discussed when power-based association scheme is deployed. Our numerical simulations are presented to demonstrate high accuracy and versatility of our mathematical model.

Chapter 5 summarizes the thesis and contributions. In addition, some future works related to our current research are also suggested.

Chapter 2

Background of Stochastic Geometry for Analyzing Cellular based IoT Network

In this chapter, we provide some mathematical preliminaries on the stochastic geometry for modeling wireless networks. First, we review different point processes and their realization. Then, we discuss about analyzing the performance of a cellular based IoT network using stochastic geometry.

2.1 Stochastic Geometry

Stochastic geometry addresses random spatial patterns [38]. Spatial patterns refers to the organization and placement of objects. Spatial patterns are observed everywhere in real world. For example, on a city-wide scale, the study of spatial patterns would include where educational organizations are located, how many of a particular type of schools (elementary, college, university) are present, and where the schools are located in relation to each other and to residential areas. Different schools can be visualized as different objects. Thus, the study of spatial patterns is important and time-worthy. Random points are the most basic and important objects in spatial pattern. Hence, the heart of stochastic geometry mainly focuses on the study of random point process. The advantages of stochastic geometry is that it analyzes the statistical properties of random collection of points, and hence, it makes random point process-based models more tractable.

2.2 Point Processes

Point process can be defined as a random collection of points is a $\mathbf{d}$-dimensional space $\mathbb{R}^{\mathbf{d}}$. In this work, we consider a 2-dimensional space $\mathbb{R}^{\mathbf{2}}$. Loosely, in most popular applications of point processes, each point represents the time or location or count of a particular event. The location of lightning strike in earth can be modelled as point process. In communication, the number of calls arriving in each minute can be modelled as point process. Some major types of point process, those are used to characterize different types of events, are discussed below.

2.2.1 Poisson Point Process

Poisson point process is one of the most important point processes because of its tractability and versatile use [39]. In PPP, the number points existing in area $A \subset \mathbb{R}^2$ $(0 < |A| < \infty)$ is a Poisson random variable. Moreover in PPP, number of points in disjoint area are independent. In particular, PPP is the stochastic process where events occur independently of one another. Page view request per day in a website is an example of PPP, where the number of arrival of requests follows Poisson distribution.

Poisson distribution can be defined as a discrete probability distribution which refers to the probability of a number of events occurring independently in a known period of time with a given average. A PPP can be expressed as $\phi = \{x_i'; i' = 1, 2, 3, \cdots\}$, where $x_{i'}$ is the location of i'^{th} node. If the given average is expressed as λ in units $\frac{\text{points}}{m^2}$, for a PPP in area $A \subset \mathbb{R}^2$ $(0 < |A| < \infty)$, the number of points, $P(A) = |\phi \cap A| \sim Poisson(\lambda)$ [40, 41]. Hence, in 2-dimensional space $\mathbb{R}^{\mathbf{2}}$, the probability mass function (PMF), i.e., probability of number of points $P(A)$ is equal to n, of PPP can be written as

$$\mathbb{P}\{P(A) = n\} = \frac{(\lambda A)^n \, e^{-(\lambda A)}}{n!}. \tag{2.1}$$

A PPP can be homogeneous or non-homogeneous. In homogeneous PPP complete randomness is assumed with a single parameter called intensity, i.e., random number of points with intensity λ are distributed randomly

and uniformly in a given set. Here, the number of points in two disjoint sets are independent. In non-homogeneous PPP the random number of points are unevenly distributed according to the intensity function. However, the independence between disjoint sets should hold in non-homogeneous PPP. In this work, we focus on homogeneous PPP distribution. A realization of homogeneous PPP is shown in Fig. 2.1

2.2.2 Point Cluster Process

PCP is generated by taking stationary PPP distributed parent point process and offspring point processes, and then translating the daughter processes to the position of their parent. Hence, PCP is obtained by applying independent clustering to PPP [40, 42]. In PCP the parent points form a stationary PPP, $\psi_p = \{x_1, x_2, x_3, \cdots\}$ with intensity $\lambda_p > 0$, i.e., the number of parent points per unit area is λ_p. The offspring points, which are also called children points, form independent PPP, denoted as ψ_c, around parent points $x_{i'}$, where $i' = 1, 2, 3, \cdots$, with intensity $\lambda_{ch} > 0$. The cluster process is the union of all offspring points. So the complete cluster process, ψ can be written as

$$\psi \equiv \cup_{x \in \psi_p} \{x + \mathbb{N}^x\}, \tag{2.2}$$

where $\mathbb{N}^x$ denotes the offspring point process around parent $x_{i'}$.

2.2.3 Matérn Cluster Process

MCP is a special type of PCP where the children points form independent PPP, ψ_c with intensity λ_{ch} in a disk of radius R_{th}, centred at $x_{i'}$ (denoted by $D(x_{i'}, R_{\text{th}})$ where $x_{i'}$ is the parent point's location), around the parent. The parent points $\{x\}$ are distributed according to homogeneous PPP with intensity λ_p. The complete clustering according to MCP, ψ can be written as $x + c = z \in \psi \equiv \cup_{x \in \psi_p} \{x + \mathbb{N}^x\}$, where $\{c\} \equiv \mathbb{N}^x$ denotes the offspring point process. The elements in z are conditionally independent and identically distributed (i.i.d.) having probability density function (PDF) $f_z(z|x)$ [43]. MCP has three parameters λ_p, λ_{ch}, and R_{th}. Hence, MCP is an isotropic and stationary PCP formed by offspring/children points

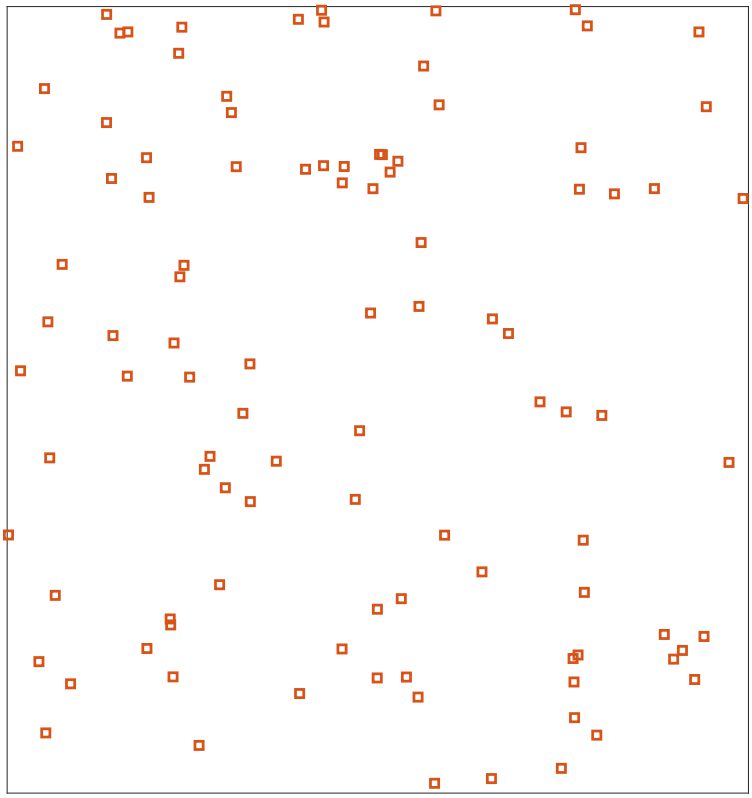

Figure 2.1: A realization of homogeneous PPP.

whose locations around the parent points are i.i.d. with the density function, $f_M(\cdots)$, expressed as

$$f_M(c) = \begin{cases} \frac{1}{\pi R_{\text{th}}^2}; ||c|| \leq R_{\text{th}}, \\ 0; \quad \text{otherwise}, \end{cases} \tag{2.3}$$

where $||c||$ is the distance of any children point related to its parent point and $||.||$ denotes Euclidean norm. A realization of MCP is shown in Fig. 2.2.

2.2.4 Thomas Cluster Process

In TCP, like any other PCP, parent points are distributed in an area $A \subset \mathbb{R}^2$ $(0 < |A| < \infty)$ according to a homogeneous PPP $\{x_1, x_2, x_3, \cdots\}$ (denoted as ψ_p) with density λ_p. Around these parent points, children points are distributed according to a symmetric normal distribution, denoted by ψ_c, with variance σ_v^2. Let us denote $\mathbb{N}_x$ is the set of offspring points for the cluster which is centred at $x \in \psi_p$. The number of children points per cluster, i.e., around a parent point, is Poisson distributed with mean $\tilde{m}$. The PDF $f_Y(y)$ of a children point location $y \subset \mathbb{R}^2$ relative to its parent point is given as [32, 44]

$$f_Y(y) = \frac{1}{2\pi\sigma_v^2} \exp\left(-\frac{y^T y}{2\sigma_v^2}\right), \qquad y \subset \mathbb{R}^2. \tag{2.4}$$

A realization of TCP is shown in Fig. 2.3.

2.3 Performance Metric

As mentioned earlier, in IoT network with manifold devices, one important step is to establish connection among the devices and their intended BSs. It is important to measure the probability of a reference device of establishing connection with its intended BS. Hence, the main performance metric of this work is connection failure probability in each time slot, which can be defined as the probability that a device is failed to connect to its in-

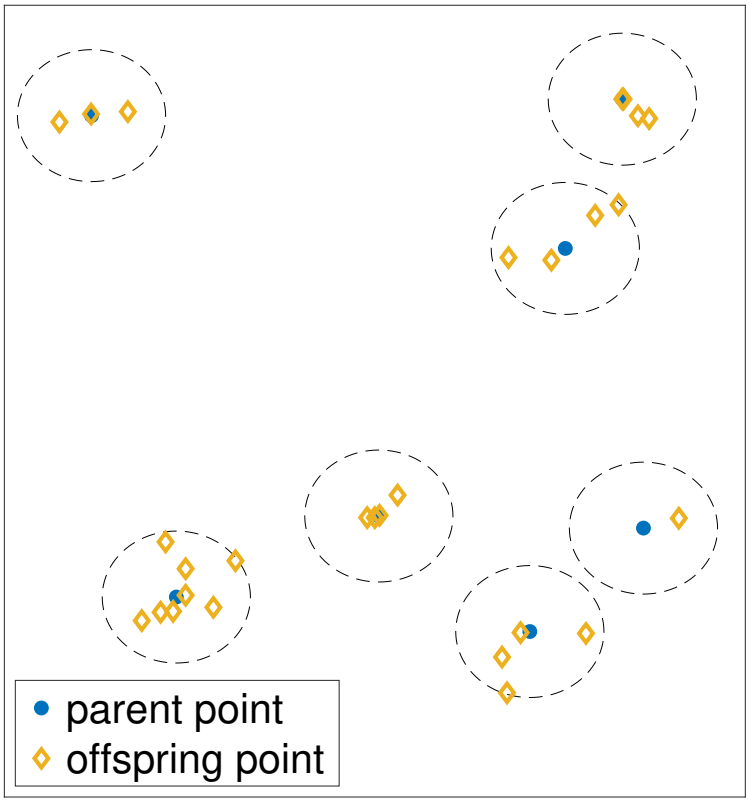

Figure 2.2: A realization of MCP.

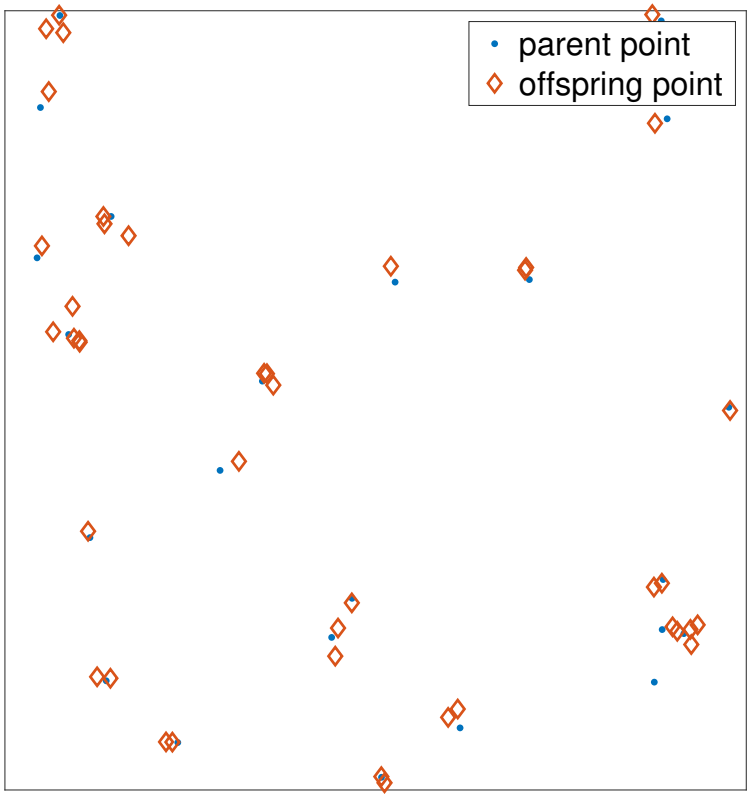

Figure 2.3: A realization of TCP.

tended BS, i.e., the SINR is below a certain threshold. If a device has failed to connect to its intended BS in a given time slot, it will continue sending a RACH request in the following time slots. SINR, γ below the threshold value, θ leads to connection failure for the device. The value of θ can be selected depending on different modulation schemes and channel capacity. Probability of failure is then written as [24]

$$\mathscr{P}_f = \mathbb{P}[\gamma < \theta], \tag{2.5}$$

where, $\mathbb{P}[x]$ denotes the probability of x. The SINR is given by

$$\begin{aligned} \gamma &= \frac{P_r}{\sigma^2 + I_{agg}} \\ &= \frac{P_t h r^{-\eta}}{\sigma^2 + I_{agg}}, \end{aligned} \tag{2.6}$$

where P_r is the received signal power, σ^2 is the noise power, I_{agg} is the aggregate interference power, P_t is the transmitted signal power, h is random channel gain, r is the distance between the device and intended BS, and η is path-loss exponent[1]. In eq. (2.6) exponential path loss model is considered. The path loss model is valid when the distance, r is in the 'far-field' of the antenna, i.e., distance $r > \frac{2D_a}{\lambda}$. Here D_a is the maximum linear dimension of the antenna and λ is the wavelength of the electro-magnetic wave.

Since we are considering UL transmission, the aggregate interference power can be expressed as the summation of powers from all interfering devices. Interference is a stochastic process which depends on the location of random devices and random fading channel gain. In RACH phase, more than one device intend to connect with one BS, and hence, interference generates from both types of devices, intended to connect with same BS as the reference device and different BSs. A realization of how the interference is generated is shown in Fig. 2.4.

Using stochastic geometry interference can be characterized by its den-

[1]The value of η, usually, varies from 2-6. For cellular radio communication in urban area η varies from 3 to 5.

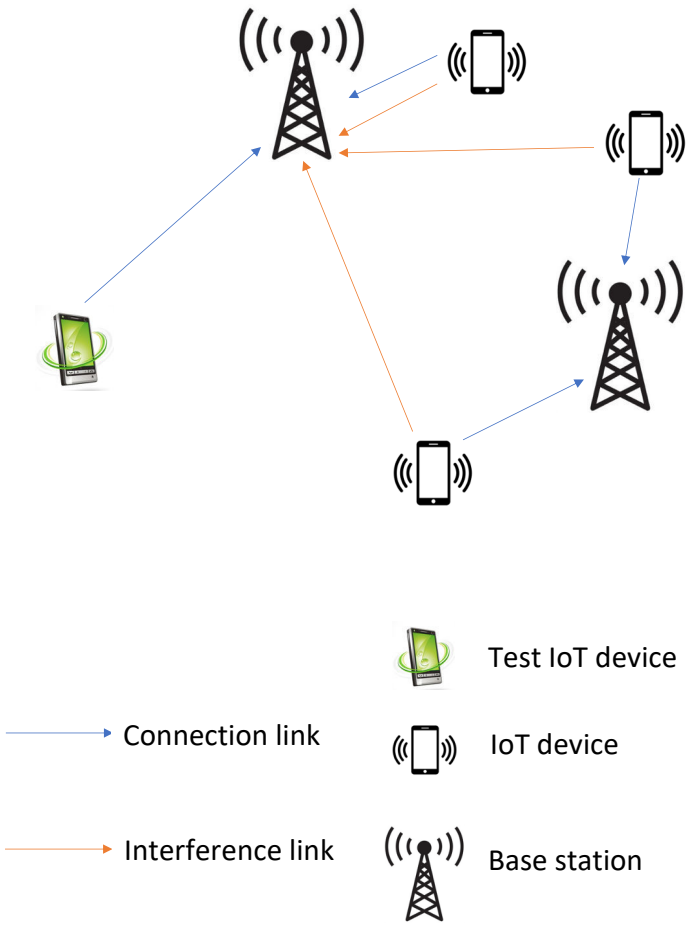

Figure 2.4: A realization of interference from IoT devices to BS.

sity function. The expression for density function of interference is unknown for large scale network [27]. Hence the interference is usually characterized by Laplace transform of its density function. Laplace transform of density function of random variable X is, hereafter, mentioned as the Laplace transform of X. Laplace transform of X can be characterized by its moment-generating function (MGF). MGF of a random variable is an alternative specification of density function, which can be characterized using stochastic geometry. Mathematically, MGF can be expressed as two-sided Laplace transform. The moment generating function of random variable X, $\mathbb{M}_X(\cdots)$ is given as

$$\mathbb{M}_X(t) = \int_{-\infty}^{\infty} f_X(x) e^{tx} dx = \mathbb{E}\left[e^{tX}\right], \qquad t \in \mathbb{R}, \tag{2.7}$$

where, $\mathbb{E}[z]$ is the expectation of random variable z and $f_X(x)$ is the density function of random variable X. Hence, the Laplace transform of X can be written as [41, 45]

$$\mathcal{L}_X(s) = \int_{0}^{\infty} f_X(x) e^{-xs} dx = \mathbb{E}\left[e^{-sX}\right]. \tag{2.8}$$

Laplace transform of interference is useful to calculate the connection failure probability mentioned in eq. (2.5). Depending on the random channel gain, the expression of $\mathscr{P}_f$ can be obtained. Rayleigh fading channel is usually assumed for its analytical tractability. In this work, we consider Rayleigh fading channel which makes h exponentially distributed. Using eqs. (2.5) and (2.6), $\mathscr{P}_f$ can be calculated as

$$\begin{aligned}
\mathscr{P}_f &= \mathbb{P}\left[h < \frac{\theta}{\rho}(\sigma^2 + I_{intra} + I_{inter})\right] \\
&= 1 - \mathbb{P}\left[h \geq \frac{\theta}{\rho}(\sigma^2 + I_{intra} + I_{inter})\right] \\
&= 1 - \mathbb{E}\left[\exp\left\{-\frac{\theta}{\rho}(\sigma^2 + I_{intra} + I_{inter})\right\}\right] \\
&= 1 - \exp\left\{-\frac{\sigma^2\theta}{\rho}\right\} \mathcal{L}_{I_{inter}}\left\{\frac{\theta}{\rho}\right\} \mathcal{L}_{I_{intra}}\left\{\frac{\theta}{\rho}\right\},
\end{aligned} \tag{2.9}$$

where, $\mathcal{L}_X\{s\}$ denotes the Laplace transform of random variable X which can be found in eq. (2.8). Note that, the intra-cell interference and the inter-cell interference are independent of each other.

Chapter 3

Performance Analysis of Single-Tier Cellular Based IoT Network

In this chapter, we focus on analyzing the performance measure of cellular network for massive connectivity of IoT devices considering three different distributions of BSs for single-tier networks. In particular, we develop a generalized approach to calculate connection failure probability of IoT devices in the RACH phase of UL transmission. The proposed approach uses a calculation of the devices' association probability rather than using an approximation of the Voronoi tessellation's cells area distribution that is used in PPP. The merit of the proposed approach besides its exact analysis, is that it can be applied for general scenarios of devices and BSs' distributions. Presented numerical results[2] demonstrate the effectiveness and accuracy of the proposed approach.

3.1 System Model

In order to describe the system model, we consider the RACH phase of a single-tier UL cellular network, where the devices are distributed according to PPP, and BSs are considered to be distributed according to

- case 1: PPP,
- case 2: children points of MCP, and

[2]Colour version of the figures, in this chapter, are available in the online copy.

– case 3: children points of TCP.

3.1.1 Network and Propagation Model

The system model with three different BSs' distribution can be described as below.

First, we consider that the BSs are distributed in an area $A \subset \mathbb{R}^2$ ($0 < |A| < \infty$) according to a homogeneous PPP, denoted by $\psi_{\rm c}$, with intensity $\lambda_{\rm BS}$.

Second, we consider that BSs are distributed according to children points of MCP. The parent points of MCP are distributed in an area $A \subset \mathbb{R}^2$ ($0 < |A| < \infty$) according to a homogeneous PPP $\{x_1, x_2, x_3, \cdots\}$ (denoted as ψ_p) with intensity λ_p. A set of BSs are distributed according to PPP, denoted as $\psi_c = \{c_b; b = 1, 2, 3, \cdots\}$, with intensity λ_{ch} within a cluster centered at $x_{i'} \subset \psi_p$ around the parent point $x_{i'}$ in the circle of radius $R_{\rm th}$; hence BSs are the children points of MCP. The intensity of BSs in the whole area A is $\lambda_{\rm BS} = \pi R_{\rm th}^2 \lambda_{ch} \lambda_p$.

Third, we consider that the BSs are distributed according to children points of TCP. The parent points of TCP are distributed in an area $A \subset \mathbb{R}^2$ ($0 < |A| < \infty$) according to a homogeneous PPP $\{x_1, x_2, x_3, \cdots\}$ (denoted as ψ_p) with intensity λ_p around which children points are distributed according to a symmetric normal distribution, denoted by ψ_c, with variance σ_v^2. The number of points per cluster, i.e., around each parent point, is Poisson distributed with mean $\tilde{m}$. Hence, BSs are the children points of TCP. The intensity of BSs in the whole area A is $\lambda_{\rm BS} = \lambda_p \tilde{m}$. For all the different cases of BSs' distribution, devices are distributed according to a homogeneous PPP, denoted as $\phi_D = \{u_i; i = 1, 2, 3, \cdots\}$, with intensity λ_u. Realizations of the system models are shown in Figs. 3.1, 3.2, and 3.3. Note that, the BSs from same service provider, more likely, form a cluster. Hence, considering the base stations to be distributed according to PCP is more practical.

We consider an exponential path-loss model, where the transmitted power decays with a rate $d^{-\eta}$ where d is the distance from device to desired BS

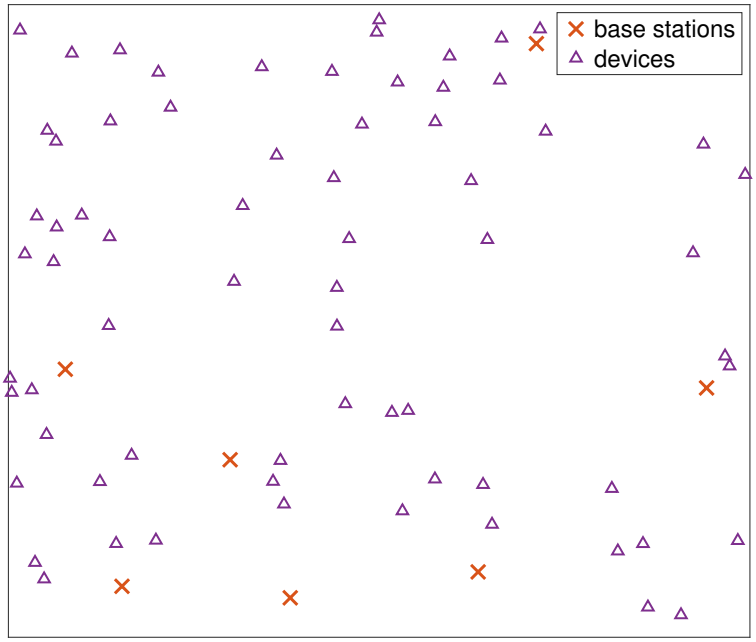

Figure 3.1: A realization of system model, where devices and BSs are distributed according to PPP.

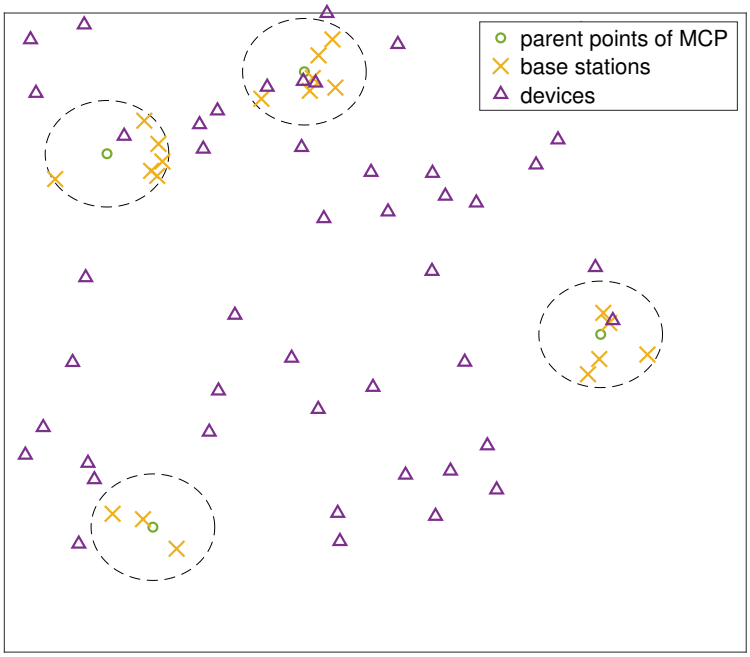

Figure 3.2: A realization of system model, where devices are distributed according to PPP, and BSs are distributed according to children points of MCP.

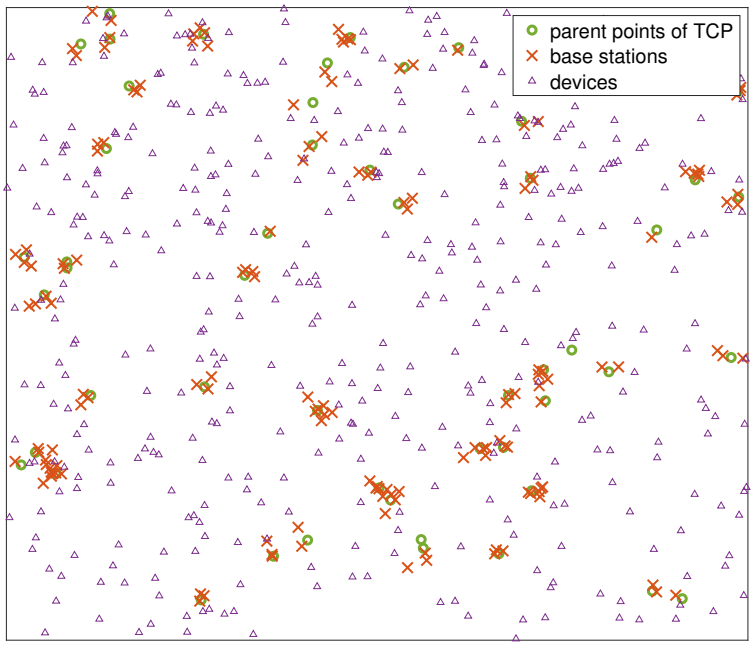

Figure 3.3: A realization of system model, where devices are distributed according to PPP, and BSs are distributed according to children points of TCP.

(propagation distance) and η is the path loss exponent. In addition to the path-loss attenuation, Rayleigh fading for multi-path environment is assumed. We denote the intended channel power gain by h and interfering channel power gain by g (i.e., h and g are exponentially distributed with unity mean). All channel gains are assumed to be independent of each other, independent of the spatial locations, and are identically distributed.

3.1.2 RACH Access

To request channel access, each device randomly and independently transmits its request on one of the available prime-length Zadoff-Chu (ZC) sequences defined by the LTE physical random access channel (PRACH) preamble. An interesting property of ZC sequences is that, the cyclically shifted versions of themselves are orthogonal to each other. It is assumed that the network is dense so that there are always multiple active devices in each BS using the same ZC sequence requesting resource allocations. Without loss of generality, we assume that all BSs have the same number of ZC sequences and that different ZC codes are orthogonal. Moreover, we assume that devices interfering on the same ZC code constitute a PPP $\tilde{\phi} \subset \phi$ with intensity $\tilde{\lambda}_u = \frac{\lambda_u}{n_Z}$, where n_Z is the number of available ZC sequences for each BS. Fig. 3.4 illustrates how the orthogonal sequences are allocated to the BSs for i'^{th} cluster. All other clusters will follow the same assignment trend.

For association of the devices to BSs, we assume that each device sends RACH access request to the nearest BS. In addition, each device uses full-inversion power control, i.e., it adjusts its transmit power P_i as such the average received power at the connected BS will be equal to a predefined threshold ρ. After a device failed to connect with the intended BS in a time slot, it continues to send RACH access request in the following time slots until it makes a successful attempt.

Our objective is to calculate the RACH access failure probability for each time slot which is defined as the probability that the SINR is lower than a given threshold. This probability is derived in the section 3.2.

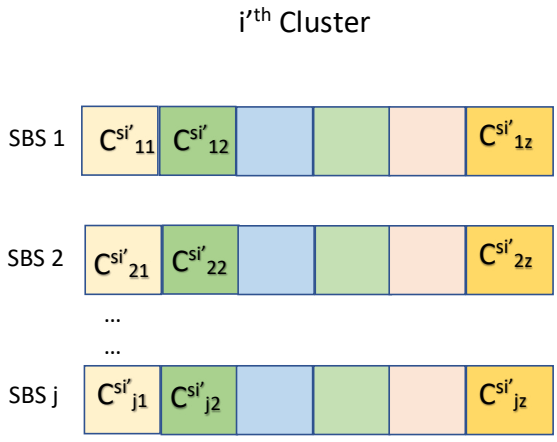

Figure 3.4: Assignment of orthogonal ZC sequences for i'^{th} cluster. Each BS has n_Z number of orthogonal codes. Different colour represents different ZC codes. $C_{jz}^{si'}$ indicates this z^{th} ZC code is associated with j^{th} BS of i'^{th} cluster.

3.2 Mathematical Analysis

3.2.1 Failure Probability

The connection failure probability corresponds to the probability of failure to obtain RACH access in each time slot. So, it is defined as the probability that a device is failed to connect to its intended BS, i.e., the SINR is below a certain threshold. Let us use γ to denote SINR and θ to denote the SINR threshold, i.e, the required SINR to connect with intended BS. Probability of failure is then written as [24]

$$\mathscr{P}_f = \mathbb{P}[\gamma < \theta], \tag{3.1}$$

where, $\mathbb{P}[x]$ denotes the probability of x. The SINR is given by

$$\gamma = \frac{\rho h}{\sigma^2 + I_{intra} + I_{inter}}, \tag{3.2}$$

where ρ is the received power threshold, h is the fading channel gain from the device to its intended BS, and σ^2 is the noise power, while I_{intra} and I_{inter} represent the intra-cell and inter-cell interference powers, respectively, which will be discussed in detail in Section 4.2.3.

Since h is exponentially distributed, using eqs. (3.1) and (3.2), $\mathscr{P}_f$ can be calculated as

$$\mathscr{P}_f = 1 - \exp\left\{-\frac{\sigma^2\theta}{\rho}\right\} \mathcal{L}_{I_{inter}}\left\{\frac{\theta}{\rho}\right\} \mathcal{L}_{I_{intra}}\left\{\frac{\theta}{\rho}\right\}, \tag{3.3}$$

where, $\mathcal{L}_X\{s\}$ denotes the Laplace transform of random variable X which is defined in eq. (2.8).

3.2.2 Laplace Transform of Interference

3.2.2.1 Inter-cell interference

The inter-cell interference, I_{inter}, is the aggregate interference coming from devices in other cells, i.e., devices connected to different BSs. Since each

device is connected to its closest BS, and the transmit power is adjusted such that the received power at the connecting BS is equal to ρ, the interference from an inter-cell interfering device is always strictly less than ρ. Thus, I_{inter} can be formulated as

$$I_{inter} = \sum_{u_i \in \phi_D \setminus \{0\}} \mathbb{1}_{P_i ||u_i||^{-\eta} < \rho} P_i g_i ||u_i||^{-\eta}, \tag{3.4}$$

where $||u_i||$ is the Euclidean norm of the distance between the interfering device to the intended BS of reference device. In eq. (3.4), $\mathbb{1}_E$ is the indicator function of event E. Following [12, 24] the Laplace transform of eq. (3.4) is obtained as

$$\mathcal{L}_{I_{inter}}(s) = \exp\left(-2\pi\tilde{\lambda}_u s^{\frac{2}{\eta}} \mathbb{E}_P[P^{\frac{2}{\eta}}] \int_{(s\rho)^{\frac{-1}{\eta}}}^{\infty} \frac{y}{y^\eta + 1} dy\right), \tag{3.5}$$

where $\mathbb{E}_x[.]$ is the expectation with respect to the random variable x. In eq. (3.5), $\mathbb{E}_P[P^{\frac{2}{\eta}}]$ is obtained by following [Lemma 1,[46]]. While deriving the moments of transmit power, we consider the fact that the transmit power of IoT device is sufficient for uplink path-loss inversion, without violating its own maximum transmit power constraint [34]. For our single-tier network where BSs are distributed according to PPP, $\mathbb{E}_P[P^{\frac{2}{\eta}}]$ can be obtained as

$$\mathbb{E}_P[P^{\frac{2}{\eta}}] = \frac{\rho^{\frac{2}{\eta}}}{\pi\ \lambda_{\text{BS}}}. \tag{3.6}$$

For the second case of BSs' distribution, where the BSs are distributed according to children points of MCP, $\mathbb{E}_P[P^{\frac{2}{\eta}}]$ can be obtained as

$$\mathbb{E}_P[P^{\frac{2}{\eta}}] = \frac{\rho^{\frac{2}{\eta}}}{\pi\ \lambda_{\text{BS}}} = \frac{\rho^{\frac{2}{\eta}}}{\pi(\lambda_p \lambda_{ch} \pi R_{th}^2)}. \tag{3.7}$$

For the third case of BSs' distribution, where the BSs are distributed

according to children points of TCP, $\mathbb{E}_P[P^{\frac{2}{\eta}}]$ can be obtained as

$$\mathbb{E}_P[P^{\frac{2}{\eta}}] = \frac{\rho^{\frac{2}{\eta}}}{\pi\ \lambda_{\text{BS}}} = \frac{\rho^{\frac{2}{\eta}}}{\pi(\lambda_p \tilde{m})}. \tag{3.8}$$

3.2.2.2 Intra-cell interference

The intra-cell interference is the aggregate interference coming from all the devices connected to the same BS of the reference device. Since all devices adjust their power such that the received power is equal to ρ, the intra-cell interference conditioned on number of neighbours n, is given by

$$I_{intra|\mathcal{N}_c=n} = \sum_{k=1}^{n} \rho g, \tag{3.9}$$

where $\mathcal{N}_c$ is the distribution of the number of devices connected to the same BS. As the devices are distributed according to PPP, the Laplace transform of intra-cell interference is given by

$$\mathcal{L}_{I_{intra}}(s) = \ \sum_{n=0}^{\infty} \frac{(\tilde{\lambda}_u\ \mathscr{A}_c\ A)^n\ \exp(-\tilde{\lambda}_u\ \mathscr{A}_c\ A)}{n!\ (1+s\rho_m)^{n\mathscr{A}_c}}, \tag{3.10}$$

where $\mathscr{A}_c$ is the probability that a typical device is connected to its nearest BS namely, association probability which in detailed in section 3.2.3.

3.2.3 Association Probaility

In order to calculate $\mathcal{L}_{I_{intra}}(s)$ in eq. (3.10), we first need to calculate $\mathscr{A}_c$. We define the distance from a typical device to its nearest BS as r_u and the distance from a typical device to v^{th} BS as r_v, where $v \in \{1, 2, \cdots V\}$. Hence, $\mathscr{A}_c$ is derived as

$$\mathscr{A}_c = \mathbb{E}\big[\mathbb{P}[r_u < \min_{v, v\neq u} r_v]\big] \tag{3.11}$$

$$= \int_0^{\infty} \mathbb{P}(\psi_c(D(O, r_u)) = 0) r_u dr_u, \tag{3.12}$$

where $\mathbb{P}(\psi_c(D(O, r_u)) = 0)$ denotes the probability that BS from ψ_c is closer than the BS at distance r_u from the typical device. Hence, this is the void probability of BS in the circular area with radius r_u around the device. It is clear that the void probability depends on the distribution of BSs. Association probability for different distributions of BSs are shown below.

3.2.3.1 PPP distributed BSs

For PPP distribution the void probability is well defined. The probability that there is no point from a PPP distribution ϕ_r of intensity λ_r within a distance Z from a reference point at O can be expressed as

$$\mathbb{P}(\phi_r(D(O, Z)) = 0) = \exp(-\lambda_r \pi Z^2). \tag{3.13}$$

Hence, for single-tier network, where BSs are distributed according to PPP, eq. (3.12) can expressed as

$$\mathscr{A}_c = \frac{1}{2\pi\lambda_{BS}}. \tag{3.14}$$

3.2.3.2 MCP distributed BSs

The void probability of children points of MCP in distance r_u can be written as

$$\begin{aligned}
&\mathbb{P}(\psi_c(D(O, r_u)) = 0) = \\
&\exp\Bigg(-2\pi\lambda_p \Bigg(\int_0^{R_{\text{th}}} \Bigg[1 - \exp\Bigg[-\lambda_{ch}\pi R_{\text{th}}^2 \Bigg(\frac{(\min(r_u, R_{\text{th}} - x))^2}{R_{\text{th}}^2} \\
&+ I_1(x, r_u) \Bigg) \Bigg] \Bigg] x dx + \int_{R_{\text{th}}}^{\infty} \Bigg[1 - \exp\Bigg(-\lambda_{ch}\pi R_{\text{th}}^2 I_2(x, r_u) \Bigg) \Bigg] x dx \Bigg) \Bigg).
\end{aligned} \tag{3.15}$$

Proof. Detailed derivation of eq. (3.15) is given in Appendix A. We also define lower bound for eq. (3.15). Then, we derive eq. (3.15) in a closed form for a given range of distance. □

Hence, for single-tier network, where BSs are distributed according to children points of MCP, (3.12) can expressed as

$$\mathscr{A}_c = \int_0^{\infty} \exp\Bigg(- 2\pi\lambda_p \Bigg(\int_0^{R_{\text{th}}} \Bigg[1 - \exp\Bigg[- \lambda_{ch}\pi R_{\text{th}}^2 \Bigg(\frac{(\min(r_u, R_{\text{th}} - x))^2}{R_{\text{th}}^2} + I_1(x, r_u) \Bigg) \Bigg] \Bigg] x dx + \int_{R_{\text{th}}}^{\infty} \Bigg[1 - \exp\Bigg(- \lambda_{ch}\pi R_{\text{th}}^2 I_2(x, r_u) \Bigg) \Bigg] x dx \Bigg) \Bigg) r_u dr_u. \tag{3.16}$$

3.2.3.3 TCP distributed BSs

The void probability of children points of TCP in distance r_u can be written as

$$\mathbb{P}(\psi_c(D(O, r_u)) = 0) = \exp\left[-2\pi\lambda_p \int_0^{\infty} \left[1 - \left(\exp\left(-\tilde{m} \left(1 - Q_1(\frac{q}{\sigma_v}, \frac{r_u}{\sigma_v}) \right) \right) \right) \right] q dq \right], \tag{3.17}$$

where $Q_1(a, b)$ is the first order *Marcum-Q-function*.

Proof. Detailed derivation of eq. (3.17) is given in Appendix B. □

Hence, for single-tier network, where BSs are distributed according to children points of TCP, (3.12) can expressed as

$$\mathscr{A}_c = \int_0^{\infty} \exp\left[-2\pi\lambda_p \int_0^{\infty} \left\{ 1 - \left(\exp\left(-\tilde{m} \left(1 - Q_1(\frac{q}{\sigma_v}, \frac{r_u}{\sigma_v}) \right) \right) \right) \right\} q dq \right] r_u dr_u. \tag{3.18}$$

3.3 Numerical Results and Discussion

In our presented scenarios, we consider a network over an area of 100 km^2. The collected statistics are taken for IoT devices located within 1 km from the origin in order to avoid the edge effects. Unless otherwise stated, we set the network parameters as follows: $n_Z = 60$ ZC sequences/BS,

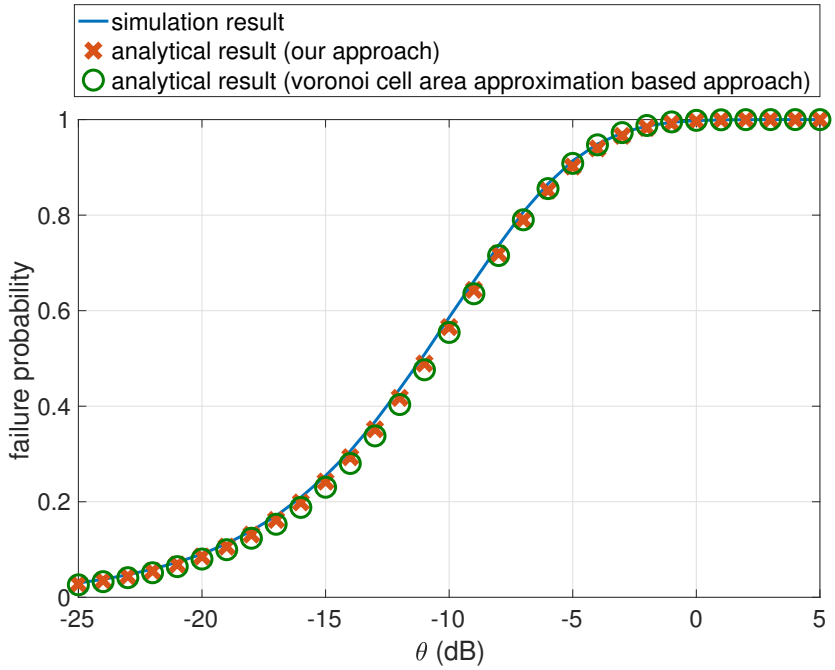

Figure 3.5: Failure probability versus SINR threshold θ for single-tier UL network where BSs are distributed according to PPP.

$\lambda_u = 12n_Z$ per km^2, $\eta = 4$, $\sigma^2 = -90$ dBm. We vary the target SINR threshold, θ from -25 to 5 dB. We set the MCP parameters, $\lambda_p = 1$ per km^2, $\lambda_{ch} = \frac{3}{\pi}$ per km^2, and $R_{\text{th}} = 1$ km. Hence, it makes $\lambda_{\text{BS}} = 3$ per km^2. For TCP parameters we set, $\lambda_p = 1$ per km^2, $\tilde{m} = 3$ per km^2, and $\sigma_v^2 = 1$. Hence, for TCP, it makes $\lambda_{\text{BS}} = 3$ per km^2. For PPP, we set the parameter, $\lambda_{\text{BS}} = 3$ per km^2.

In Fig. 3.5, we plot the failure probability versus target SINR threshold using our approach for a single-tier network where BSs are distributed according to PPP. In order to compare our approach and the Voronoi cell area approximation based calculation, in this figure, we also plot the connection failure probability using the approach in [24]. This figure shows that our proposed approach is more accurate than the Voronoi cell area approximation based approach. In Figs. 3.6 and 3.7 we plot the failure probability

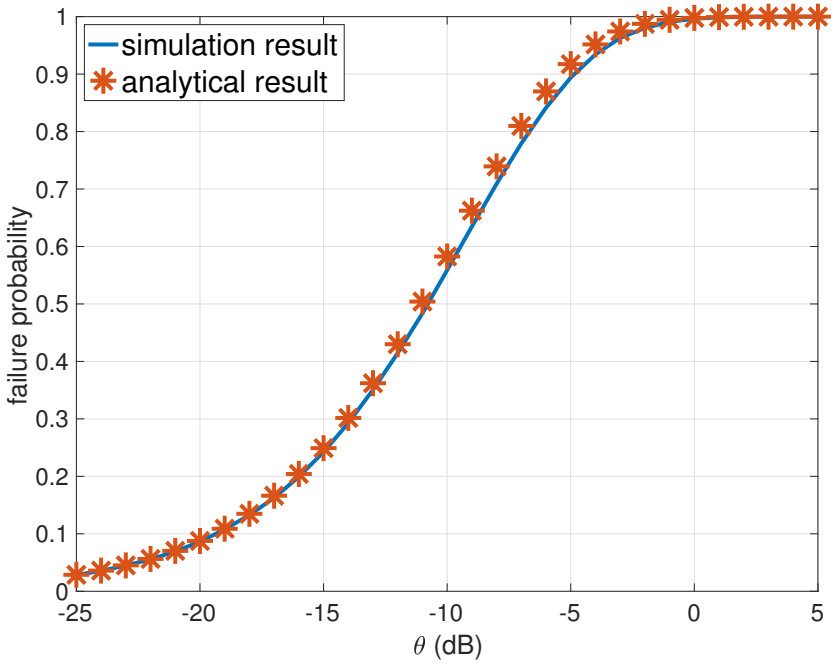

Figure 3.6: Failure probability versus SINR threshold θ for single-tier UL network where BSs are distributed according to MCP.

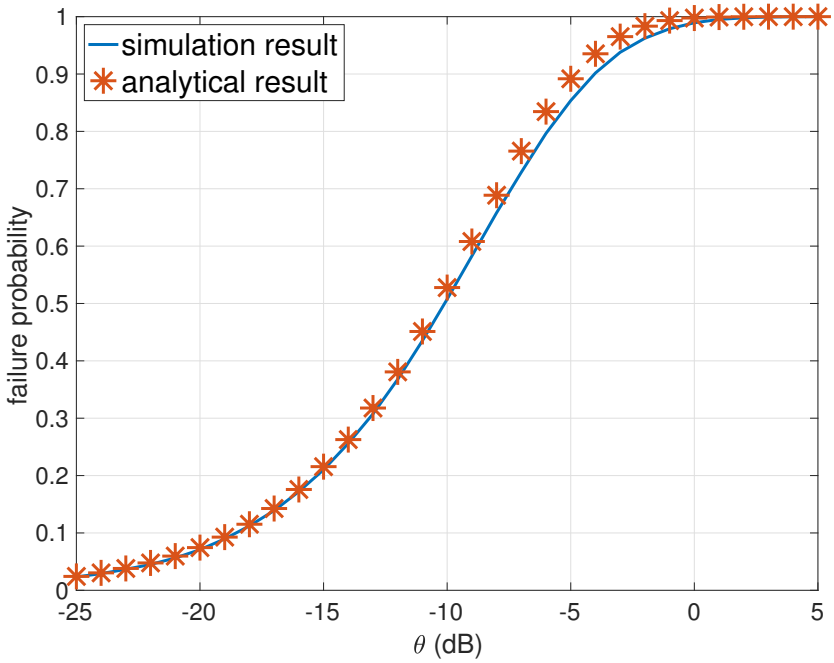

Figure 3.7: Failure probability versus SINR threshold θ for single-tier UL network where BSs are distributed according to TCP.

versus target SINR threshold where BSs are distributed according to MCP and TCP rspectively. From these figure, it is obvious that the analytical results are in agreement with the simulation results which are obtained using Monte Carlo method. We also observe that for all cases, the failure probability increases as the SINR threshold increases, as expected.

One of the main objectives of our performance derivation is to study how to ensure a certain failure probability for given SINR requirement and devices' intensity. As such network designer can set values of various design parameters. Thus, in Figs. 3.8, 3.9, and 3.10, we show the failure probability for different ratio of the devices and BS' intensities ($\frac{\lambda_u}{\lambda_{\text{BS}}}$). From these figures, one can estimate the required intensity of the deployed BSs, λ_{BS} for given values of θ, devices intensity, λ_u, and connection failure probability. For example, from Fig. 3.9, if we fix the SINR threshold $\theta = -20$ dB and

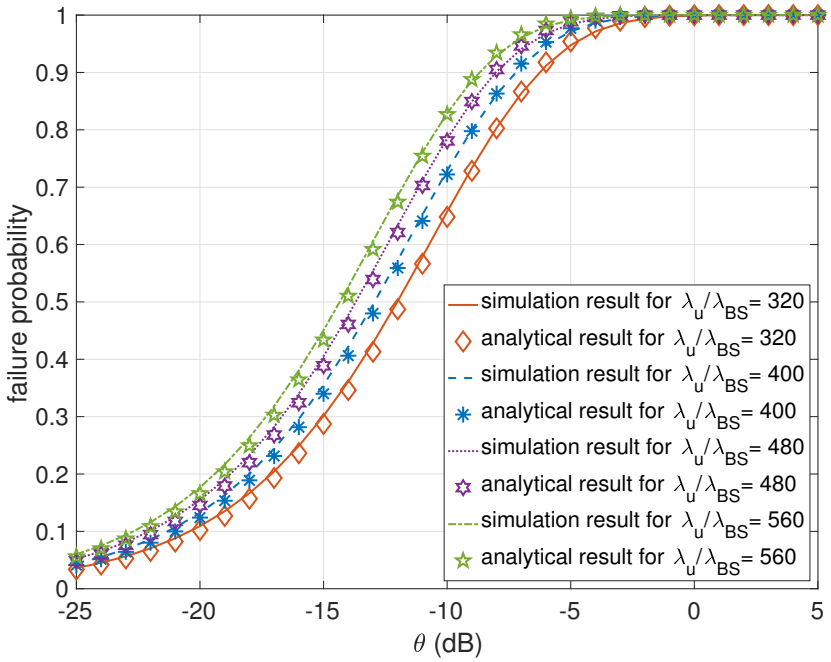

Figure 3.8: Failure probability for different $\frac{\lambda_u}{\lambda_{\text{BS}}}$, where $\lambda_{\text{BS}} = 3$ per km^2, $\lambda_u = 16n_Z, 20n_Z, 24n_Z, 28n_Z$ per km^2, and BSs are distributed according to PPP.

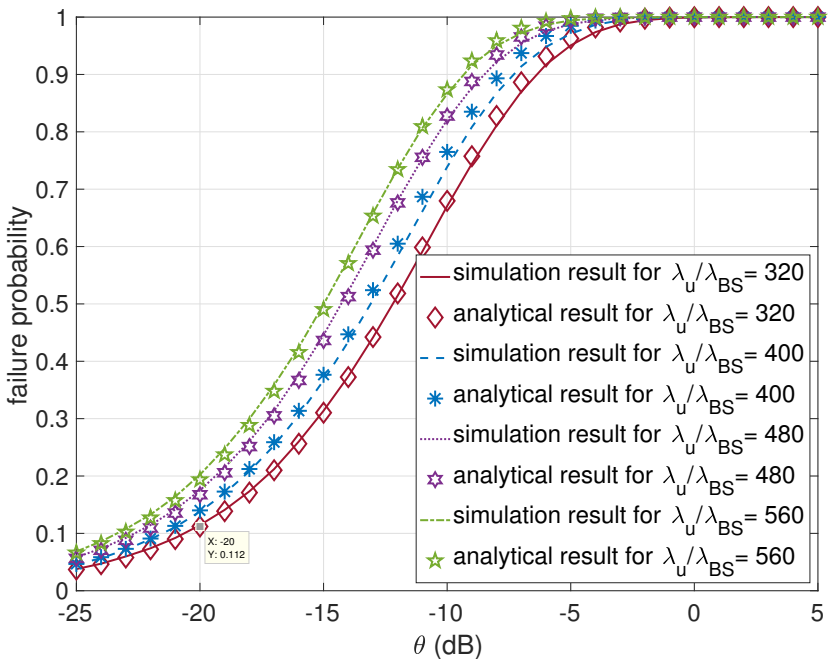

Figure 3.9: Failure probability for different $\frac{\lambda_u}{\lambda_{\text{BS}}}$, where $\lambda_{\text{BS}} = 3$ per km^2, $\lambda_u = 16n_Z, 20n_Z, 24n_Z, 28n_Z$ per km^2, and BSs are distributed according to MCP.

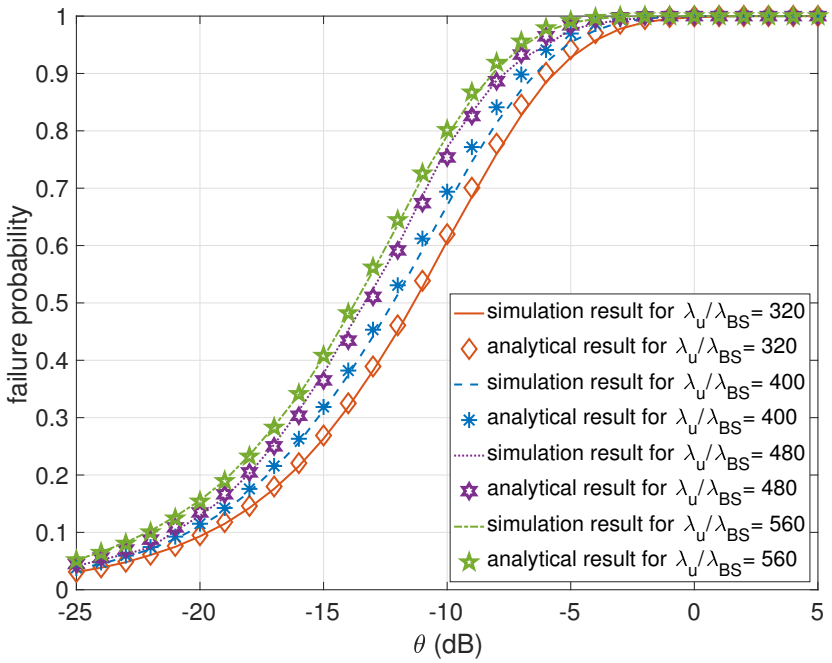

Figure 3.10: Failure probability for different $\frac{\lambda_u}{\lambda_{\text{BS}}}$, where $\lambda_{\text{BS}} = 3$ per km^2, $\lambda_u = 16n_Z, 20n_Z, 24n_Z, 28n_Z$ per km^2, and BSs are distributed according to TCP.

we want to ensure the failure probability to be less than 12% in a network model where BSs are distributed according to single-tier MCP, the intensity of the devices should be maximum 320 times of the intensity of BSs while 60 orthogonal ZC sequences are associated with a BS. These figures also confirms the trend of saturation of the network with the increase of the devices' intensity.

In order to calculate the failure probability, we derive the void probability for MCP and TCP in Appendix A and B. In this section, we also validate the analytical expressions for void probability using simulation results. In Fig. 3.11, we plot the void probability versus distance to validate our derived void probability for MCP in eq. (A.8). The figure depicts that the analytical result converges with the simulation result. We plot void probability for different cluster size. The figure clearly shows that the void probability decreases as the value of R_{th} increases. This is due to the reason that when the value of R_{th} increases, more BS are deployed in a given area. As such, a typical device has a higher probability to find for a BS within a smaller area.

In Fig. 3.12, we plot our derived lower bound for void probability using eq. (A.12) for different values of R_{th}. In this figure, we also plot the exact void probability. From this figure, we can observe that the lower bound becomes tighter when the value of R_{th} is higher. The reason can be explained as follows. For very high value of R_{th}, $I_1(x, Z)$ and $I_2(x, Z)$ become significantly low. On the other hand, $1 - exp(-y) \approx y$ for very small value of y. Hence, with these two facts it is obvious that for very high value of R_{th}, $\mathbb{P}_L(\psi_c(D(O, Z)) = 0) \approx \mathbb{P}(\psi_c(D(O, Z)) = 0)$. From this figure, we also observe that the lower bound is valid for any range of R_{th} and Z. Such an observation is mathematically expected as well. In Fig. 3.13, we plot the approximate void probability using eq. (A.13) for different values of R_{th}. Since this approximation is only valid for the range: $Z \leq \frac{R_{\text{th}}}{2}$, we have plotted this approximation only for this range. This figure shows there is a negligible difference between the approximation and the exact void probability in the given range.

In Fig. 3.14, we plot the void probability versus distance to validate

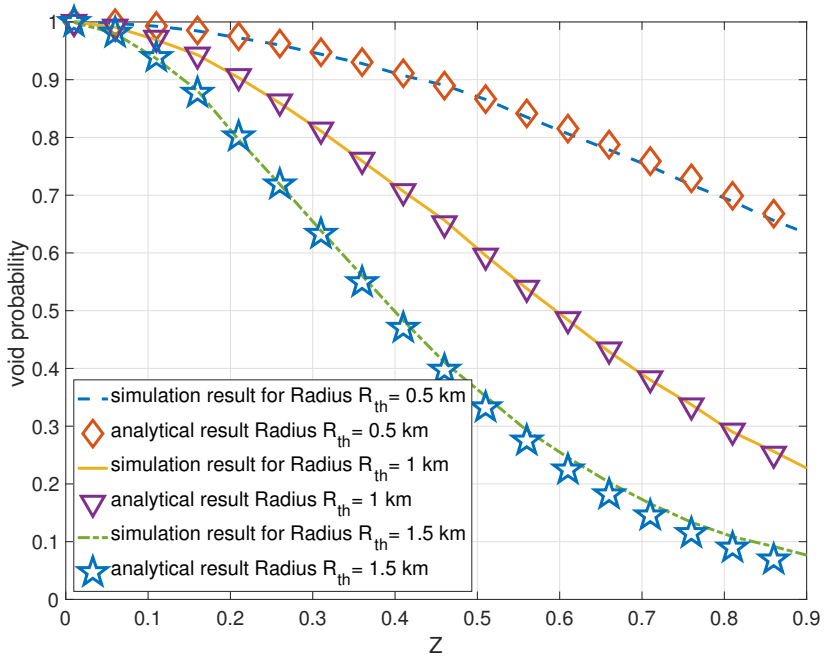

Figure 3.11: Void probability versus distance Z for various cluster radius R_{th}, where $\lambda_p = 1$ per km^2 and $\lambda_{ch} = 3$ per km^2.

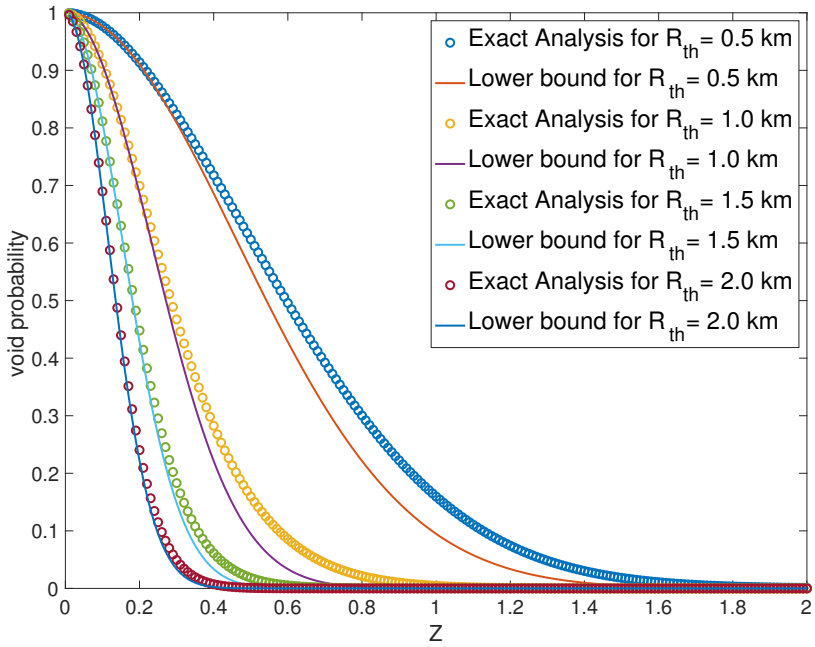

Figure 3.12: Void probability versus distance Z for exact analysis in eq. (A.8) and lower bound in eq. (A.12) for any value of Z, where $\lambda_p = 1$ per km^2 and $\lambda_{ch} = 3$ per km^2.

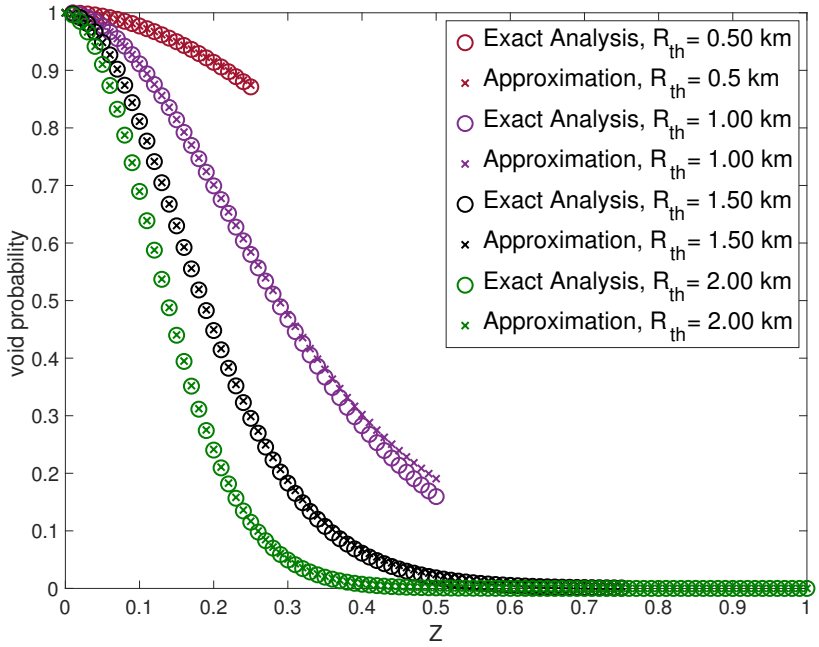

Figure 3.13: Void probability versus distance Z for exact analysis in eq. (A.8) and the approximation eq. (A.13) for $0 \leq Z \leq \frac{R_{\text{th}}}{2}$, where $\lambda_p = 1$ per km^2 and $\lambda_{ch} = 3$ per km^2.

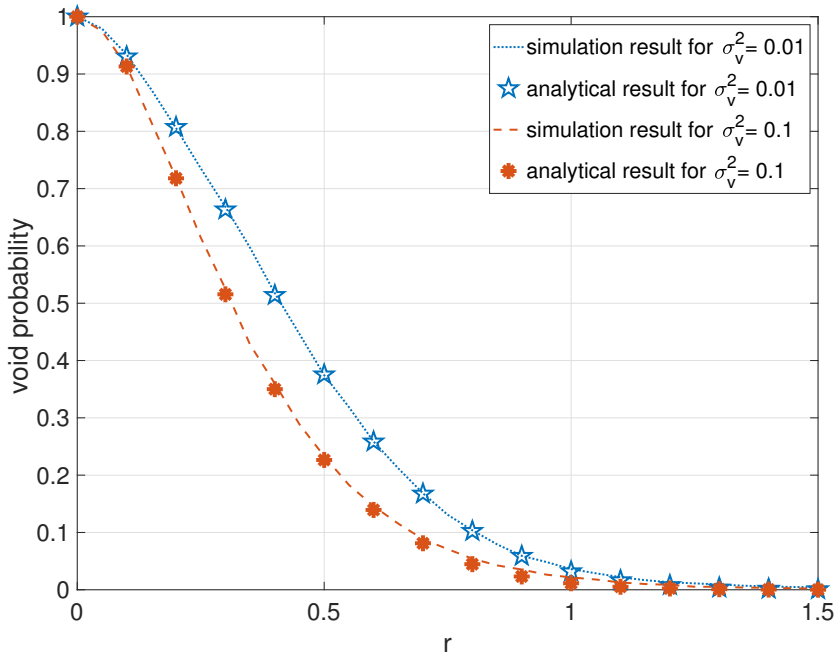

Figure 3.14: Void probability versus distance r for TCP, where $\lambda_p = 1$ per km^2, $\tilde{m} = 3$ per cluster, and $\sigma_v^2 = 0.01, 0.1$.

our derived void probability for TCP in eq. (B.6). The figure depicts that the analytical result converges with the simulation result. We plot void probability for different value variance, which is the scattering factor of the offspring points. The figure clearly shows that the void probability decreases as the value of σ_v^2 increases. This is due to the reason that when the value of σ_v^2 increases, BS are deployed in a wider area. As such, a typical device has a higher probability to find for a BS within a smaller area.

3.4 Summary

Exploiting stochastic geometry, in this chapter, we have developed a novel mathematical approach to calculate connection failure probability in each time slot for cellular based single-tier UL IoT network. Presented numerical results have demonstrated that our approach is accurate and adaptable for general scenarios of BSs' distribution. As demonstrated via example applications, the presented analysis provides engineering insights that can assist network designers to tune various design parameters to meet certain connection failure probability.

Chapter 4

Performance Analysis of Multi-Tier Cellular Based IoT Network

In Chapter 3, we have developed a novel and generalized mathematical approach for calculating failure probability in each time slot in RACH access phase considering IoT enabled single-tier cellular networks. In this chapter we introduce a generalized approach to calculate the delay and failure probability for each time slot in RACH access phase considering multi-tier cellular based IoT networks. For association, we consider two different device association schemes, namely, *distance threshold-based association* and *power-based association*. We derive mathematical model for different distributions of BSs to show the adoptability of our approach. Finally, we present some selected numerical examples[3] to show the accuracy of our derived expressions.

4.1 System Model

Our proposed approach, to calculate connection failure probability, can be adopted for multi-tier networks; however, for simplicity we consider a two-tier network. We consider that the devices are distributed according to PPP, and BSs are distributed according to

- case 1: PPP,
- case 2: parents and children points of MCP, and

[3]Colour version of the figures, in this chapter, are available in the online copy.

– case 3: parents and children points of TCP.

4.1.1 Network and Propagation Model

As mentioned earlier, we consider three different distributions of BSs which are described below.

First, we consider that the MBSs and SBSs are distributed in an area $A \subset \mathbb{R}^2$ $(0 < |A| < \infty)$ according to a homogeneous PPP, denoted by ψ_{p} and ψ_{c} respectively, with intensity λ_{MBS} and λ_{SBS}.

Second, the MBSs are distributed in an area $A \subset \mathbb{R}^2$ $(0 < |A| < \infty)$ according to a homogeneous PPP $\{x_1, x_2, x_3, \cdots\}$ (denoted as ψ_p) with density $\lambda_p = \lambda_{MBS}$, and these points are the parent points (cluster centres) of the MCP. A set of SBSs are distributed according to PPP, denoted as $\psi_c = \{c_b; b = 1, 2, 3, \cdots\}$, with density λ_{ch} within a cluster centered at $x_{i'} \subset \psi_p$ around the parent point $x_{i'}$ in the circle of radius R_{th}; hence, SBSs are the children points of MCP. The intensity of SBS in the whole area A is $\lambda_{SBS} = \pi R_{\mathrm{th}}^2 \lambda_{ch} \lambda_p$.

Third, we consider that MBSs are distributed in an area $A \subset \mathbb{R}^2$ $(0 < |A| < \infty)$ according to a homogeneous PPP $\{x_1, x_2, x_3, \cdots\}$ (denoted as ψ_p) with density $\lambda_p = \lambda_{MBS}$. These points are the parent points of the TCP around which children points are distributed according to a symmetric normal distribution, denoted by ψ_c, with variance σ_v^2. The number of points per cluster, i.e., around per parent point, is Poisson distributed with mean $\tilde{m}$. Hence, SBSs are the children points of TCP. The intensity of SBSs in the whole area A is $\lambda_{\mathrm{SBS}} = \lambda_p \tilde{m}$. For all the different cases of BSs' distribution, devices are distributed according to a homogeneous PPP, denoted as $\phi_D = \{u_i; i = 1, 2, 3, \cdots\}$, with intensity λ_u. Realizations of the system models are shown in Figs. 4.1, 4.2, and 4.3.

We consider an exponential path-loss model where the received power decays with a rate $d^{-\eta}$ where d is the distance from device to desired BS (propagation distance) and η is the path loss exponent. In addition to the path-loss attenuation, Rayleigh fading for multi-path environment is assumed [24, 25]. We denote the intended channel power gain by h_k and

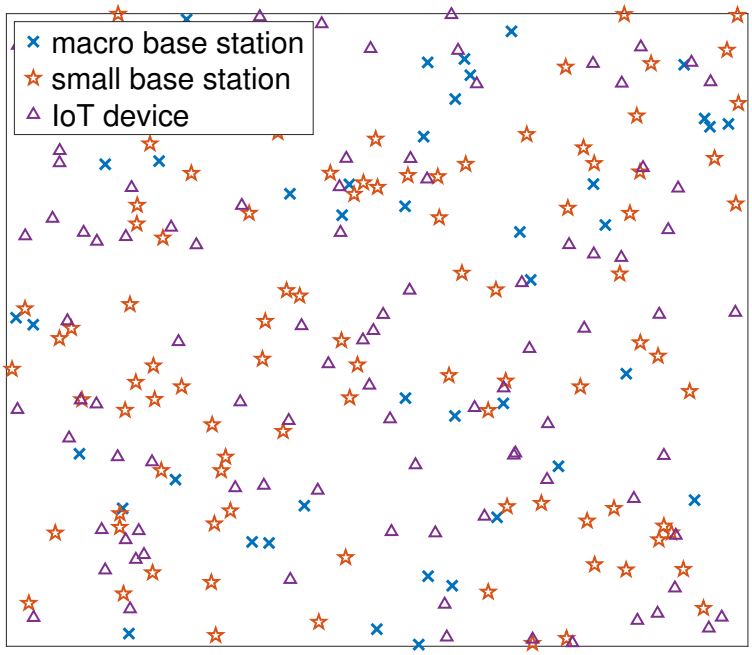

Figure 4.1: A realization of system model, where devices, SBSs and MBSs are distributed according to PPP.

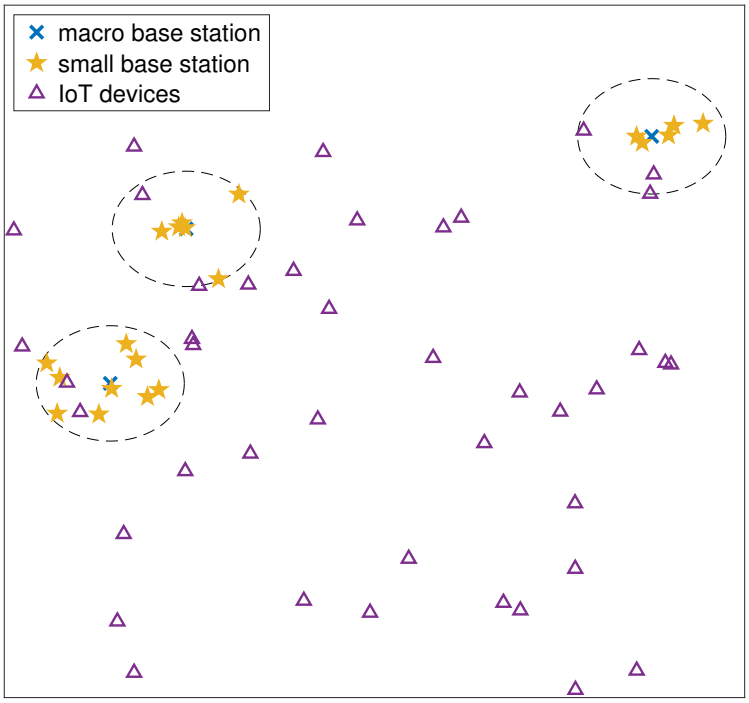

Figure 4.2: A realization of system model, where devices are distributed according to PPP, and MBSs and SBSs are distributed according parents and children points of TCP.

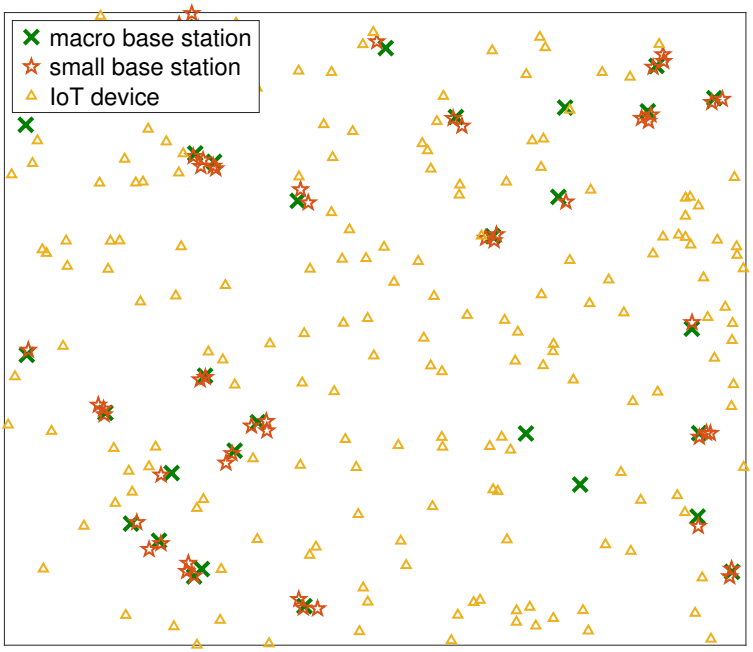

Figure 4.3: A realization of system model, where devices are distributed according to PPP, and MBSs and SBSs are distributed according parents and children points of TCP.

interfering channel power gain by g_k for k^{th} tier (i.e., h_k and g_k are exponentially distributed with unity mean). All channel gains are assumed to be independent of each other, independent of the spatial locations, and are identically distributed.

4.1.2 Association Schemes

For association of the devices to BSs we consider two schemes: (i) *distance threshold-based association*, and (ii) *power-based association*. For *distance threshold-based association* [35], it is considered that if there is any SBS within a certain distance threshold D_{th} from the device, the device will be connected to the nearest SBS. Otherwise, it will be connected to the nearest MBS. Tuning this threshold value the traffic load in a given tier, can be controlled. In other words, D_{th} is a load balancing parameter. For example, if the the threshold distance, $D_{\text{th}} = 0$, all devices will be connected to the MBSs which corresponds to a single-tier PPP network. For *power-based association*, a particular device will be connected to the BS for which it has to transmit the lowest amount of power.

4.1.3 RACH Access

To request channel access, each device in the cluster randomly and independently transmits its request on one of the available prime-length Zadoff-Chu (ZC) sequences, defined by the LTE physical random access channel (PRACH) preamble. It is assumed that there are always multiple active devices in each BS using the same ZC sequence requesting channel access. Without loss of generality, we assume that all BSs have n_Z number of ZC codes that are orthogonal. Moreover, we assume that devices interfering on the same ZC code constitute a PPP $\tilde{\psi}_D \subset \psi_D$ with intensity $\tilde{\lambda}_u = \frac{\lambda_u}{n_Z}$.

We make similar assumption as in [24, 25] that each device uses full-inversion power control, i.e., it adjusts its transmit power $\mathcal{P}_i$ such that the average received power at the connected BS will be equal to a predefined threshold/ power control threshold ρ_k. A device sends the RACH access request to the intended BS following the aforementioned power-control law. A

successful RACH access attempt allows subsequent transmission from device to BS. The device will have an unsuccessful/failed RACH access attempt if it fails to reach the required SINR level. If the device fails to have a successful RACH access it will resend the request at the following time slot until it succeeds to establish the connection. To resend the request it will adjust its transmit power with the same power control threshold ρ_k.

Our objective is to calculate the RACH access failure probability for each time slot which is defined as the probability that the SINR is lower than a given threshold. This probability is derived in the Section 4.2. We also compute average waiting time for a successful RACH, which is a function of failure probability for each time slot.

4.2 Performance Analysis

4.2.1 Failure Probability and Delay for Successful RACH Access

Let us use γ_k to denote SINR and θ_k to denote the SINR threshold, i.e., required SINR to connect with intended BS, for k^{th} tier. Without loss of generality, we consider $\theta_k = \theta$ for all tiers. The failure probability of k^{th} tier $\mathscr{P}_{f_k}$ can be written as

$$\mathscr{P}_{f_k} = \mathbb{P}[\gamma_k < \theta], \tag{4.1}$$

where, $\mathbb{P}[x]$ denotes the probability of event x. The SINR, γ_k is expressed as

$$\gamma_k = \frac{\rho_k h_k}{\sigma^2 + I_{intra_k} + I_{inter_k}}, \tag{4.2}$$

where ρ_k is the received power threshold for k^{th} tier BS where $k \in \{m, s\}$, i.e., ρ_m and ρ_s denote the received power threshold for macro-tier and small-tier BSs, respectively. h_k denotes the fading channel gain from the device to its intended BS, and σ^2 is the noise power. I_{intra_k} and I_{inter_k} represent the intra-cell and inter-cell interferences for k^{th} tier, respectively.

Since h_k is exponentially distributed, using eqs. (4.1) and (4.2), $\mathscr{P}_{f_k}$

can be calculated as [24]

$$\mathscr{P}_{f_k} = 1 - \exp\left\{-\frac{\sigma^2\theta}{\rho_k}\right\} \mathcal{L}_{I_{inter_k}}\left\{\frac{\theta}{\rho_k}\right\} \mathcal{L}_{I_{intra_k}}\left\{\frac{\theta}{\rho_k}\right\}, \tag{4.3}$$

where, $\mathcal{L}_X\{s\}$ denotes the Laplace transform of random variable X which is defined as

$$\mathcal{L}_X(s) = \mathbb{E}[\exp\{-sX\}]. \tag{4.4}$$

Calculation of eq. (4.3) requires derivation for Laplace transform of inter-cell and intra-cell interferences which are derived in Section 4.2.3. By using $\mathscr{P}_{f_k}$ and corresponding association probability, the overall probability of connection failure can be obtained as

$$\mathscr{P}_f = \sum_{k=1}^{K} \mathscr{P}_{f_k} \mathcal{A}_k. \tag{4.5}$$

Note that, the association probability for tier k, $\mathcal{A}_k$ depends on the employed devices' association scheme[4]. For brevity, we introduce $\mathcal{A}_k^a$ to denote the association probability of k^{th} tier with association scheme $a \in \{d, p\}$ where d stands for distance threshold-based association, and p stands for power-based association. This probability corresponds to the probability that a typical device is connected to a BS in k^{th} tier for given association scenario. An IoT device will continue to submit RACH request until one successful RACH. Therefore, the average waiting time for the successful RACH, $\mathcal{D}$ is given by

$$\mathcal{D} = \frac{1}{1 - \mathscr{P}_f}. \tag{4.6}$$

In order to calculate failure probability in eq. (4.5) and correspondingly the average wait time in eq. (4.6), we need to calculate association probability $\mathcal{A}_k^a$.

[4]For ease of demonstration we consider two-tier network, i.e., $K = 2$ and $k \in \{m, s\}$.

4.2.2 Exact Calculation of Association Probability for a Given Tier, $\mathcal{A}_k^a$

The association probability for a given tier k, $\mathcal{A}_k^a$ where $k \in \{m, s\}$ and $a \in \{d, p\}$, can be defined as the probability of a typical device is associated with one BS of k^{th} tier with a given association scheme. In order to calculate the association probability, we calculate the void probability. For a given distribution ϕ_r, this probability is defined as the probability of having no points from ϕ_r in a given distance from a reference point which is not a part of ϕ_r.

4.2.2.1 Distance threshold-based association

With the distance threshold-based association, a typical device

a. will be connected to the nearest MBS if there is no SBS at distance D_{th} from the user,

b. will be connected to nearest SBS if the nearest SBS is in distance D_{th} from the user.

The probability of having no point from point process ψ_c in a disk of radius D_{th} having the device in the centre; which is denoted by $\mathbb{P}(\psi_c(D(O, D_{\text{th}})) = 0)$. So, the association probability of tier of MBS with distance threshold-based association $\mathcal{A}_m^d$ can be written as

$$\mathcal{A}_m^d(D_{\text{th}}) = \mathbb{P}(\psi_c(D(O, D_{\text{th}})) = 0), \tag{4.7}$$

where a device is situated at point O. Since a particular device will be associated with either MBS or SBS, the association probability of tier of SBS $\mathcal{A}_s^d$ can be written as

$$\mathcal{A}_s^d(D_{\text{th}}) = 1 - \mathcal{A}_m^d(D_{\text{th}}). \tag{4.8}$$

Hence, the association probability for a given tier is a function of void probability of the respective distribution. Association probabilities for macro-tier and small tier, for the three different distributions of BSs, are discussed below.

4.2.2.1.1 PPP distributed BSs: The void probability for PPP is given in eq. (3.13). For this case, where both MBSs and SBSs are distributed according to PPP, the association probability of tier of MBS with distance threshold-based association $\mathcal{A}_m^d$ can be written as

$$\begin{aligned}\mathcal{A}_m^d(D_{\text{th}}) &= \mathbb{P}(\psi_c(D(O, D_{\text{th}})) = 0) \\ &= \exp(-\lambda_{\text{SBS}}\pi D_{\text{th}}^2).\end{aligned} \tag{4.9}$$

Hence, the association probability of the tier of SBS $\mathcal{A}_s^d$ can be written as

$$\mathcal{A}_s^d(D_{\text{th}}) = 1 - \exp(-\lambda_{\text{SBS}}\pi D_{\text{th}}^2). \tag{4.10}$$

4.2.2.1.2 MCP distributed BSs: The void probability of children points of MCP is given in eq. (A.8). For this case, where MBSs and SBSs are distributed according to parents and children points of MCP, the association probability of tier of MBS with distance threshold-based association $\mathcal{A}_m^d$ can be written as

$$\begin{aligned}&\mathcal{A}_m^d(D_{\text{th}}) = \mathbb{P}(\psi_c(D(O, D_{\text{th}})) = 0) \\ &= \exp\Bigg(- 2\pi\lambda_p \Bigg(\int_0^{R_{\text{th}}} \Bigg[1 - \exp\Bigg[- \lambda_{ch}\pi R_{\text{th}}^2 \Bigg(\frac{(\min(D_{\text{th}}, R_{\text{th}} - x))^2}{R_{\text{th}}^2} \\ &+ I_1(x, D_{\text{th}}) \Bigg) \Bigg] \Bigg] x dx + \int_{R_{\text{th}}}^{\infty} \Bigg[1 - \exp\Bigg(- \lambda_{ch}\pi R_{\text{th}}^2 I_2(x, D_{\text{th}}) \Bigg) \Bigg] x dx \Bigg) \Bigg),\end{aligned} \tag{4.11}$$

where $I_1(x, D_{\text{th}})$ and $I_2(x, D_{\text{th}})$ are given in eqs. (A.9) and (A.10). Hence, the association probability of the tier of SBS $\mathcal{A}_s^d$ can be written as

$$\begin{aligned}&\mathcal{A}_s^d(D_{\text{th}}) = \\ &1 - \exp\Bigg(- 2\pi\lambda_p \Bigg(\int_0^{R_{\text{th}}} \Bigg[1 - \exp\Bigg[- \lambda_{ch}\pi R_{\text{th}}^2 \Bigg(\frac{(\min(D_{\text{th}}, R_{\text{th}} - x))^2}{R_{\text{th}}^2}\end{aligned}$$

$$+ I_1(x, D_{\text{th}})\Big)\Big]\Big] x dx + \int_{R_{\text{th}}}^{\infty} \Big[1 - \exp\Big(- \lambda_{ch}\pi R_{\text{th}}^2 I_2(x, D_{\text{th}})\Big)\Big] x dx\Big)\Big). \tag{4.12}$$

4.2.2.1.3 TCP distributed BSs: The void probability of children points of TCP is given in eq. (B.6). For this case, where MBSs and SBSs are distributed according to parents and children points of TCP, the association probability of tier of MBS with distance threshold-based association $\mathcal{A}_m^d$ can be written as

$$\begin{aligned}&\mathcal{A}_m^d(D_{\text{th}}) = \mathbb{P}(\psi_c(D(O, D_{\text{th}})) = 0)\\ &= \exp\left[-2\pi\lambda_p \int_0^{\infty} \left\{1 - \left(\exp\left(-\tilde{m}\left(1 - Q_1(\frac{q}{\sigma_v}, \frac{D_{th}}{\sigma_v})\right)\right)\right)\right\} q dq\right],\end{aligned} \tag{4.13}$$

where where $Q_1(a, b)$ is the first order *Marcum-Q-function*. . Hence, the association probability of the tier of SBS $\mathcal{A}_s^d$ can be written as

$$\begin{aligned}&\mathcal{A}_s^d(D_{\text{th}}) =\\ &1 - \exp\left[-2\pi\lambda_p \int_0^{\infty} \left\{1 - \left(\exp\left(-\tilde{m}\left(1 - Q_1(\frac{q}{\sigma_v}, \frac{D_{th}}{\sigma_v})\right)\right)\right)\right\} q dq\right].\end{aligned} \tag{4.14}$$

4.2.2.2 Power-based association

For this association scheme a typical device will be connected to the BS for which it requires the lowest amount of power. A typical device will be associated with k^{th} tier when the transmit power to connect with a BS in k^{th} tier is lower than the transmit power to connect to all other BSs in all j^{th} tier, i.e., $\rho_k R_k^{\eta} < \rho_j R_j^{\eta}$ where $j \in \{1, 2, \cdots K\}$ considering total number of tiers is K, R_k and R_j is the minimum distance from the typical user to the BS of k^{th} tier and j^{th} tier, respectively; whereas for two-tier network we define R_m and R_s as the minimum distance from the typical user to the BS of macro-tier and small-tier, respectively. Then, association probability for

k^{th} tier can be derived as

$$\begin{aligned}\mathcal{A}_k^p &= \mathbb{E}_{R_k}\big[\mathbb{P}[\rho_k R_k^\eta \ < \ \min_{j,j\neq k} \rho_j R_j^\eta]\big] \\ &= \mathbb{E}_{R_k}\big[\prod_{j=1,j\neq k}^{K} \mathbb{P}[\rho_k R_k^\eta \ < \ \rho_j R_j^\eta]\big] \\ &= \mathbb{E}_{R_k}\big[\prod_{j=1,j\neq k}^{K} \mathbb{P}[R_j \ > \ (\frac{\rho_k}{\rho_j})^{\frac{1}{\eta}} R_k]\big] \\ &= \int_0^\infty \prod_{j=1,j\neq k}^{K} \mathbb{P}[R_j \ > \ (\frac{\rho_k}{\rho_j})^{\frac{1}{\eta}} r_k] f_{R_k}(r_k) dr_k. \end{aligned} \tag{4.15}$$

In eq. (4.15), $\mathbb{P}[R_j \ > \ (\frac{\rho_k}{\rho_j})^{\frac{1}{\eta}} r_k]$ is the void probability of j^{th} tier BS in the circular area with radius $(\frac{\rho_k}{\rho_j})^{\frac{1}{\eta}} r_k$ around the device. For two-tier network, from eq. (4.15), association probability in macro-tier and small-tier can be written as

$$\mathcal{A}_m^p((\frac{\rho_m}{\rho_s})^{\frac{1}{\eta}}) = \int_0^\infty \mathbb{P}(\psi_c(D(O,((\frac{\rho_m}{\rho_s})^{\frac{1}{\eta}} r_m))) = 0) f_{R_m}(r_m) dr_m, \tag{4.16}$$

$$\mathcal{A}_s^p((\frac{\rho_m}{\rho_s})^{\frac{1}{\eta}}) = 1 - \mathcal{A}_m^p((\frac{\rho_m}{\rho_s})^{\frac{1}{\eta}}), \tag{4.17}$$

where $\mathbb{P}(\psi_c(D(O,(\frac{\rho_m}{\rho_s}^{\frac{1}{\eta}} r_m))) = 0)$ is void probability for point process ψ_c in the circular area of radius $(\frac{\rho_m}{\rho_s})^{\frac{1}{\eta}} r_m$ around the device. Hence, the calculation of $\mathbb{P}(\psi_c(D(O,(\frac{\rho_m}{\rho_s}^{\frac{1}{\eta}} r_m))) = 0)$ depends on the distribution of ψ_c. For all different cases of BSs' distribution, the MBSs are always considered to be PPP distributed, so $f_{R_m}(r_m)$ can be written as

$$f_{R_m}(r_m) = 2\pi r_m \ \lambda_{\text{MBS}} \exp(-\pi r_m^2 \lambda_{\text{MBS}}). \tag{4.18}$$

Hence, the association probability for macro-tier, $\mathcal{A}_m^p((\frac{\rho_m}{\rho_s})^{\frac{1}{\eta}})$ and small-tier, $\mathcal{A}_s^p((\frac{\rho_m}{\rho_s})^{\frac{1}{\eta}})$ for different distributions of BSs are shown below.

4.2.2.2.1 PPP distributed BSs: For this case, where both MBSs and SBSs are distributed according to PPP, the association probability for macro-tier, $\mathcal{A}_m^p((\frac{\rho_m}{\rho_s})^{\frac{1}{\eta}})$ nd small-tier, $\mathcal{A}_s^p((\frac{\rho_m}{\rho_s})^{\frac{1}{\eta}})$ can be written as, respectively,

$$\begin{aligned}\mathcal{A}_m^p((\frac{\rho_m}{\rho_s})^{\frac{1}{\eta}}) &= \int_0^\infty \mathbb{P}(\psi_c(D(O,((\frac{\rho_m}{\rho_s})^{\frac{1}{\eta}} r_m))) = 0) f_{R_m}(r_m) dr_m \\ &\overset{(a)}{=} \int_0^\infty \exp(-\lambda_{\text{SBS}}\pi((\frac{\rho_m}{\rho_s})^{\frac{1}{\eta}} r_m)^2) 2\pi r_m \lambda_{\text{MBS}} \exp(-\pi r_m^2 \lambda_{\text{MBS}}) dr_m \\ &= \frac{\lambda_{\text{MBS}}}{\left(\frac{\rho_m}{\rho_s}\right)^{\frac{1}{\eta}} \lambda_{\text{SBS}} + \lambda_{\text{MBS}}}, \end{aligned} \tag{4.19}$$

$$\mathcal{A}_s^p((\frac{\rho_m}{\rho_s})^{\frac{1}{\eta}}) = \frac{\lambda_{\text{SBS}}}{\left(\frac{\rho_s}{\rho_m}\right)^{\frac{1}{\eta}} \lambda_{\text{MBS}} + \lambda_{\text{SBS}}}. \tag{4.20}$$

Here, (a) follows the void probability of PPP, which is given in eq. (3.13).

4.2.2.2.2 MCP distributed BSs: For this case, where MBSs and SBSs are distributed according to parents and children points of MCP, the association probability for macro-tier, $\mathcal{A}_m^p((\frac{\rho_m}{\rho_s})^{\frac{1}{\eta}})$ and small-tier, $\mathcal{A}_s^p((\frac{\rho_m}{\rho_s})^{\frac{1}{\eta}})$ can be written as, respectively,

$$\begin{aligned}\mathcal{A}_m^p((\frac{\rho_m}{\rho_s})^{\frac{1}{\eta}}) &= \int_0^\infty \mathbb{P}(\psi_c(D(O,((\frac{\rho_m}{\rho_s})^{\frac{1}{\eta}} r_m))) = 0) f_{R_m}(r_m) dr_m \\ &\overset{(a)}{=} \int_0^\infty \Bigg(\exp\Bigg(-2\pi\lambda_p \Bigg(\int_0^{R_{\text{th}}} \Bigg[1 - \exp\Bigg[-\lambda_{ch}\pi R_{\text{th}}^2 \\ &\quad \times \Bigg(\frac{(\min(((\frac{\rho_m}{\rho_s})^{\frac{1}{\eta}} r_m), R_{\text{th}} - x))^2}{R_{\text{th}}^2} + I_1(x, ((\frac{\rho_m}{\rho_s})^{\frac{1}{\eta}} r_m)) \Bigg) \Bigg] \Bigg] x dx \\ &\quad + \int_{R_{\text{th}}}^\infty \Bigg[1 - \exp\Bigg(-\lambda_{ch}\pi R_{\text{th}}^2 I_2(x, ((\frac{\rho_m}{\rho_s})^{\frac{1}{\eta}} r_m)) \Bigg) \Bigg] x dx \Bigg) \Bigg) \Bigg) \\ &\quad \times 2\pi r_m \lambda_{\text{MBS}} \exp(-\pi r_m^2 \lambda_{\text{MBS}}) dr_m, \end{aligned} \tag{4.21}$$

$$\mathcal{A}_s^p((\frac{\rho_m}{\rho_s})^{\frac{1}{\eta}}) = 1 - \int_0^\infty \Bigg(\exp\Bigg(-2\pi\lambda_p \Bigg(\int_0^{R_{\text{th}}} \Bigg[1 - \exp\Bigg[-\lambda_{ch}\pi R_{\text{th}}^2$$

$$\times \left(\frac{(\min(((\frac{\rho_m}{\rho_s})^{\frac{1}{\eta}} r_m), R_{\text{th}} - x))^2}{R_{\text{th}}^2} + I_1(x, ((\frac{\rho_m}{\rho_s})^{\frac{1}{\eta}} r_m)) \right) \Bigg] \Bigg] x dx$$
$$+ \int_{R_{\text{th}}}^{\infty} \left[1 - \exp\left(- \lambda_{ch} \pi R_{\text{th}}^2 I_2(x, ((\frac{\rho_m}{\rho_s})^{\frac{1}{\eta}} r_m)) \right) \right] x dx \Bigg) \Bigg) \Bigg)$$
$$\times 2\pi r_m \lambda_{\text{MBS}} \exp(-\pi r_m^2 \lambda_{\text{MBS}}) dr_m. \tag{4.22}$$

Here, (a) follows the void probability of MCP, which is given in eq. (A.8).

4.2.2.2.3 TCP distributed BSs: For this case, where MBSs and SBSs are distributed according to parents and children points of TCP, the association probability for macro-tier, $\mathcal{A}_m^p((\frac{\rho_m}{\rho_s})^{\frac{1}{\eta}})$ and small-tier, $\mathcal{A}_s^p((\frac{\rho_m}{\rho_s})^{\frac{1}{\eta}})$ can be written as, respectively,

$$\mathcal{A}_m^p \left((\frac{\rho_m}{\rho_s})^{\frac{1}{\eta}} \right) = \int_0^{\infty} \mathbb{P}(\psi_c(D(O, ((\frac{\rho_m}{\rho_s})^{\frac{1}{\eta}} r_m))) = 0) f_{R_m}(r_m) dr_m$$
$$\overset{(a)}{=} \int_0^{\infty} \exp\left[- 2\pi\lambda_p \int_0^{\infty} \left\{ 1 - \left(\exp\left(- \tilde{m} \right. \right. \right. \right.$$
$$\left. \left. \left. \left. \times \left(1 - Q_1(\frac{q}{\sigma_v}, \frac{((\frac{\rho_m}{\rho_s})^{\frac{1}{\eta}} r_m)}{\sigma_v}) \right) \right) \right) \right\} q dq \Bigg] 2\pi r_m \lambda_{\text{MBS}} \exp(-\pi r_m^2 \lambda_{\text{MBS}}) dr_m, \tag{4.23}$$

$$\mathcal{A}_s^p \left((\frac{\rho_m}{\rho_s})^{\frac{1}{\eta}} \right) = 1 - \int_0^{\infty} \exp\left[- 2\pi\lambda_p \int_0^{\infty} \left\{ 1 - \left(\exp\left(- \tilde{m} \right. \right. \right. \right.$$
$$\left. \left. \left. \left. \times \left(1 - Q_1(\frac{q}{\sigma_v}, \frac{((\frac{\rho_m}{\rho_s})^{\frac{1}{\eta}} r_m)}{\sigma_v}) \right) \right) \right) \right\} q dq \Bigg] 2\pi r_m \lambda_{\text{MBS}} \exp(-\pi r_m^2 \lambda_{\text{MBS}}) dr_m. \tag{4.24}$$

Here, (a) follows the void probability of TCP, which is given in eq. (B.6).

4.2.3 Laplace Transform of Interference

4.2.3.1 Inter-cell interference

The inter-cell interference for k^{th} tier BS, I_{inter_k}, is the aggregate interference coming from devices in the other cells, i.e., devices connected to different BSs.

4.2.3.1.1 Distance threshold-based association: For this association scheme, we consider $\rho_k = \rho$. So, according to power-control law, the transmit power of devices is adjusted such that the received power at the connecting BS is equal to ρ. The devices associated with a given tier, is connected with the nearest BS in that tier. As a result, the interference from an inter-cell interfering device associated with the same tier of the reference device is always strictly less than ρ. The interference from an inter-cell interfering device associated with other tier is less than ∞. The interfering devices, which are associated with a given tier k, constitute a PPP $\psi_D^k \subset \psi_D$ with intensity $\lambda_u^k = \mathcal{A}_k^d(D_{\text{th}})\lambda_u$, where $k \in \{m, s\}$.

Thus, if the device is associated with macro-tier, I_{inter_m} can be written as

$$I_{inter_m} = \sum_{u_i \in \psi_D^m \setminus \{0\}} \mathbb{1}_{\mathcal{P}_i ||u_i||^{-\eta} < \rho} \mathcal{P}_i g_i ||u_i||^{-\eta} + \sum_{u_i \in \psi_D^s \setminus \{0\}} \mathbb{1}_{\mathcal{P}_i ||u_i||^{-\eta} < \infty} \mathcal{P}_i g_i ||u_i||^{-\eta}, \tag{4.25}$$

where $||u_i||$ is the Euclidean norm of the distance between the interfering device to the intended BS of reference device. If the device is associated with small-tier, I_{inter_s} can be written as

$$I_{inter_s} = \sum_{u_i \in \psi_D^s \setminus \{0\}} \mathbb{1}_{\mathcal{P}_i ||u_i||^{-\eta} < \rho} \mathcal{P}_i g_i ||u_i||^{-\eta} + \sum_{u_i \in \psi_D^m \setminus \{0\}} \mathbb{1}_{\mathcal{P}_i ||u_i||^{-\eta} < \infty} \mathcal{P}_i g_i ||u_i||^{-\eta}. \tag{4.26}$$

Following [12, 24] the Laplace transform of eqs. (4.25) and (4.26) can be

obtained as, respectively,

$$\mathcal{L}_{I_{inter_m}}(s) = \exp\left(-2\pi\frac{\lambda_u^m}{n_Z}s^{\frac{2}{\eta}}\mathbb{E}^d_{\mathcal{P}_m}[\mathcal{P}_m^{\frac{2}{\eta}}]\int_{(s\rho)^{\frac{-1}{\eta}}}^{\infty}\frac{y}{y^\eta+1}dy\right), \tag{4.27}$$

$$\mathcal{L}_{I_{inter_s}}(s) = \exp\left(-2\pi\frac{\lambda_u^s}{n_Z}s^{\frac{2}{\eta}}\mathbb{E}^d_{\mathcal{P}_s}[\mathcal{P}_s^{\frac{2}{\eta}}]\int_{(s\rho)^{\frac{-1}{\eta}}}^{\infty}\frac{y}{y^\eta+1}dy\right), \tag{4.28}$$

where $\mathbb{E}^d_x[.]$ is the expectation with respect to the random variable x for distance threshold-based asscociation. In eqs. (4.27) and (4.28), $\mathbb{E}^d_{\mathcal{P}_m}[\mathcal{P}_m^{\frac{2}{\eta}}]$ and $\mathbb{E}^d_{\mathcal{P}_s}[\mathcal{P}_s^{\frac{2}{\eta}}]$ are obtained by following [Lemma 1,[46]]. While deriving the moments of transmit power, we consider the fact that the transmit power of an IoT device is sufficient for uplink path-loss inversion, without violating its own maximum transmit power constraint [34]. For different distributions of BSs $\mathbb{E}^d_{\mathcal{P}_m}[\mathcal{P}_m^{\frac{2}{\eta}}]$ and $\mathbb{E}^d_{\mathcal{P}_s}[\mathcal{P}_s^{\frac{2}{\eta}}]$ can be obtained as below.

4.2.3.1.1.1 PPP distributed BSs: For this case both MBSs and SBSs distributed according to PPP and hence, $\mathbb{E}^d_{\mathcal{P}_m}[\mathcal{P}_m^{\frac{2}{\eta}}]$ and $\mathbb{E}^d_{\mathcal{P}_s}[\mathcal{P}_s^{\frac{2}{\eta}}]$ can be obtained as

$$\mathbb{E}^d_{\mathcal{P}_m}[\mathcal{P}_m^{\frac{2}{\eta}}] = \frac{\rho^{\frac{2}{\eta}}}{\pi\lambda_{MBS}}, \tag{4.29}$$

$$\mathbb{E}^d_{\mathcal{P}_s}[\mathcal{P}_s^{\frac{2}{\eta}}] = \frac{\rho^{\frac{2}{\eta}}}{\pi\lambda_{SBS}}. \tag{4.30}$$

4.2.3.1.1.2 MCP distributed BSs: For this case MBSs and SBSs distributed according to parent and children points of MCP. Hence, $\mathbb{E}^d_{\mathcal{P}_m}[\mathcal{P}_m^{\frac{2}{\eta}}]$ and $\mathbb{E}^d_{\mathcal{P}_s}[\mathcal{P}_s^{\frac{2}{\eta}}]$ can be obtained as

$$\mathbb{E}^d_{\mathcal{P}_m}[\mathcal{P}_m^{\frac{2}{\eta}}] = \frac{\rho^{\frac{2}{\eta}}}{\pi\lambda_{MBS}} = \frac{\rho^{\frac{2}{\eta}}}{\pi\lambda_p}, \tag{4.31}$$

$$\mathbb{E}^d_{\mathcal{P}_s}[\mathcal{P}_s^{\frac{2}{\eta}}] = \frac{\rho^{\frac{2}{\eta}}}{\pi\lambda_{SBS}} = \frac{\rho^{\frac{2}{\eta}}}{\pi(\pi R_{\text{th}}^2\lambda_{ch}\lambda_p)}. \tag{4.32}$$

4.2.3.1.1.3 TCP distributed BSs: For this case MBSs and SBSs distributed according to parent and children points of MCP. Hence, $\mathbb{E}^d_{\mathcal{P}_m}[\mathcal{P}_m^{\frac{2}{\eta}}]$

and $\mathbb{E}^{d}_{\mathcal{P}_s}[\mathcal{P}_s^{\frac{2}{\eta}}]$ can be obtained as

$$\mathbb{E}^{d}_{\mathcal{P}_m}[\mathcal{P}_m^{\frac{2}{\eta}}] = \frac{\rho^{\frac{2}{\eta}}}{\pi\lambda_{MBS}} = \frac{\rho^{\frac{2}{\eta}}}{\pi\lambda_p}, \tag{4.33}$$

$$\mathbb{E}^{d}_{\mathcal{P}_s}[\mathcal{P}_s^{\frac{2}{\eta}}] = \frac{\rho^{\frac{2}{\eta}}}{\pi\lambda_{SBS}} = \frac{\rho^{\frac{2}{\eta}}}{\pi\lambda_p\tilde{m}}. \tag{4.34}$$

4.2.3.1.2 Power-based association: For power-based association scenario devices are associated with the BS for which they have to transmit the lowest power. The transmit power of devices is adjusted such that the received power at the connecting BS is equal to ρ_k. As a result, for power-based association scenario the interference from an inter-cell interfering device is always strictly less than ρ_k. So, I_{inter_k} can be written as

$$I_{inter_k} = \sum_{u_i \in \psi_D \setminus \{0\}} \mathbb{1}_{\mathcal{P}_i ||u_i||^{-\eta} < \rho_k} \mathcal{P}_i g_i ||u_i||^{-\eta}. \tag{4.35}$$

The Laplace transform of eq. (4.35) can be written as

$$\mathcal{L}_{I_{inter_k}}(s) = \exp\left(-2\pi\tilde{\lambda}_u s^{\frac{2}{\eta}} \mathbb{E}^{p}_{\mathcal{P}_k}[\mathcal{P}_k^{\frac{2}{\eta}}] \int_{(s\rho_k)^{\frac{-1}{\eta}}}^{\infty} \frac{y}{y^\eta + 1} dy\right), \tag{4.36}$$

where $\mathbb{E}^{p}_{x}[.]$ is the expectation with respect to the random variable x for power-based association. By following [Lemma 2,[46]], we derive $\mathbb{E}^{p}_{\mathcal{P}_k}[\mathcal{P}_k^{\frac{2}{\eta}}]$ for different BSs' distribution, which is shown below.

4.2.3.1.2.1 PPP distributed BSs: For this case, $\mathbb{E}^{p}_{\mathcal{P}_k}[\mathcal{P}_k^{\frac{2}{\eta}}]$ can be written as

$$\mathbb{E}^{p}_{\mathcal{P}_k}[\mathcal{P}_k^{\frac{2}{\eta}}] = \frac{\rho_k^{\frac{2}{\eta}}}{\pi(\lambda_{MBS} + \lambda_{SBS})}. \tag{4.37}$$

4.2.3.1.2.2 MCP distributed BSs: For this case, $\mathbb{E}^{p}_{\mathcal{P}_k}[\mathcal{P}_k^{\frac{2}{\eta}}]$ can be written as

$$\mathbb{E}^{p}_{\mathcal{P}_k}[\mathcal{P}_k^{\frac{2}{\eta}}] = \frac{\rho_k^{\frac{2}{\eta}}}{\pi(\lambda_{MBS} + \lambda_{SBS})} = \frac{\rho_k^{\frac{2}{\eta}}}{\pi(\lambda_p + \pi R_{\text{th}}^2 \lambda_{ch} \lambda_p)}. \tag{4.38}$$

4.2.3.1.2.3 TCP distributed BSs: For this case, $\mathbb{E}^{p}_{\mathcal{P}_k}[\mathcal{P}_k^{\frac{2}{\eta}}]$ can be written as

$$\mathbb{E}^{p}_{\mathcal{P}_k}[\mathcal{P}_k^{\frac{2}{\eta}}] = \frac{\rho_k^{\frac{2}{\eta}}}{\pi(\lambda_{MBS}+\lambda_{SBS})} = \frac{\rho_k^{\frac{2}{\eta}}}{\pi(\lambda_p+\lambda_p\tilde{m})}. \tag{4.39}$$

4.2.3.2 Intra-cell interference

The intra-cell interference is the aggregate interference coming from all the devices connected to the same BS of the reference device. So the interference coming from an individual intra-cell interfering device is equal to ρ_k considering the reference device is connected to a BS of k^{th} tier. Hence, all devices adjust their power such that the received power is equal to ρ_k, the intra-cell interference conditioned on number of neighbours n, is given by

$$I_{intra_k|\mathcal{N}_c=n} = \sum_{n'=1}^{n} \rho_k g_k, \tag{4.40}$$

where $\mathcal{N}_c$ is the distribution of the number of devices connected to the BS using same orthogonal sequence. As devices are distributed according to PPP, the Laplace transform of intra-cell interference for k^{th} tier with association scheme a is given by

$$\mathcal{L}_{I_{intra_k}}(s) \;=\; \sum_{n=0}^{\infty} \frac{(-\tilde{\lambda}_u\ \mathcal{A}_k^a\ \mathscr{A}_k\ A)^n\ \exp(-\tilde{\lambda}_u\ \mathcal{A}_k^a\ \mathscr{A}_k\ A)}{n!\ (1+s\rho_k)^{n\mathcal{A}_k^a\mathscr{A}_k}}, \tag{4.41}$$

where $\mathscr{A}_k$ is the probability that a typical device is connected to its nearest BS in a given tier k. $\mathcal{A}_k^a$ given in eq. (4.41) can be found from Section 4.2.2 for respective distribution and association scheme. As mentioned earlier, for distance threshold-based association, we consider $\rho_k = \rho$.

To calculate eq. (4.41), we need to calculate $\mathscr{A}_k$. We define the distance from a typical device to its nearest BS as r_u and the distance from a typical device to v^{th} BS in a given tier as r_v, where $v \in \{1, 2, \cdots V\}$. Hence, $\mathscr{A}_k$ can be derived as

$$\mathscr{A}_k = \mathbb{E}\big[\mathbb{P}[r_u < \min_{v, v\neq u} r_v]\big]$$

$$= \int_0^\infty \mathbb{P}[r_u < \min_{v,v\neq u} r_v] r_u dr_u, \tag{4.42}$$

where $\mathbb{P}[r_u < \min_{v,v\neq u} r_v]$ is the probability that no BS from k^{th} tier is closer than the BS at distance r_u from the typical device. Hence, this is the void probability of k^{th} tier BS in the circular area with radius r_u around the device. It is clear that the void probability depends on the distribution of BSs of a given tier. In the considered two-tier network models the MBSs PPP distributed. The void probability for PPP is given is eq. (3.13). So, the probability that a typical device is connected to its nearest BS from macro-tier, $\mathscr{A}_m$ can be obtained as

$$\mathscr{A}_m = \int_0^\infty \exp(-\lambda_{\text{MBS}} \pi r_u^2) r_u dr_u. \tag{4.43}$$

For different distributions of SBSs, the probability that a typical device is connected to its nearest BS from small-tier, $\mathscr{A}_s$ can be obtained as below.

4.2.3.2.1 SBSs are distributed according to PPP: For this case, $\mathscr{A}_s$ can be written as

$$\mathscr{A}_s = \int_0^\infty \exp(-\lambda_{\text{SBS}} \pi r_u^2) r_u dr_u. \tag{4.44}$$

4.2.3.2.2 SBSs are distributed according children points to MCP: The void probability for children points of MCP is given in eq.(A.8). So, for this case, $\mathscr{A}_s$ can be written as

$$\mathscr{A}_s = \int_0^\infty \exp\Bigg(-2\pi\lambda_p \Bigg(\int_0^{R_{\text{th}}} \Bigg[1 - \exp\Bigg[-\lambda_{ch}\pi R_{\text{th}}^2 \Bigg(\frac{(\min(r_u, R_{\text{th}} - x))^2}{R_{\text{th}}^2} + I_1(x, r_u) \Bigg) \Bigg] \Bigg] x dx + \int_{R_{\text{th}}}^\infty \Bigg[1 - \exp\Bigg(-\lambda_{ch}\pi R_{\text{th}}^2 I_2(x, r_u) \Bigg) \Bigg] x dx \Bigg) \Bigg) r_u dr_u, \tag{4.45}$$

where $I_1(x, r_u)$ and $I_2(x, r_u)$ are given in eqs. (A.9) and (A.10).

4.2.3.2.3 SBSs are distributed according children points to TCP: The void probability for children points of TCP is given in eq.(B.6). So, for this case, $\mathscr{A}_s$ can be written as

$$\mathscr{A}_s = \exp\left[-2\pi\lambda_p \int_0^{\infty} \left\{1 - \left(\exp\left(-\tilde{m}\left(1 - Q_1(\frac{q}{\sigma_v}, \frac{r_u}{\sigma_v})\right)\right)\right)\right\} q dq\right]. \tag{4.46}$$

4.3 Numerical Results and Discussion

Unless otherwise stated we consider RACH phase of a two-tier UL network, and set the network parameters as follows: $n_Z = 60$ ZC sequences per BS, $\lambda_u = 6n_Z$ per km^2, $\eta = 4$, $\sigma^2 = -90$ dBm. In our presented numerical results, we consider a network over an area of 100 km^2. The collected statistics are taken for IoT devices located within 1 km from the origin in order to avoid the edge effects. For distance threshold-based association, we consider $D_{\text{th}} = 0.8$ km and $\rho = -90$ dBm whereas for power-based association, we consider $\rho_m = -90$ dBm and $\rho_s = -100$ dBm. We vary the target SINR threshold, θ from -25 to 5 dB.

For the intensity of the MBSs, we set $\lambda_p = \lambda_{MBS} = 1$ per km^2. In case of network model where both MBSs and SBSs are distributed according to PPP, we set $\lambda_{SBS} = 3$ per km^2. For system model, where SBSs are distributed according to children points of MCP, we choose $R_{\text{th}} = 1$ km, $\lambda_{ch} = \frac{3}{\pi}$ per km^2, and hence, it makes $\lambda_{SBS} = 3$ per km^2. In order to set the intensity of the BSs in the network we define $\lambda_{BS} = \lambda_p(\pi R_{\text{th}}^2 \lambda_{ch} + 1)$. For the third considered model, where SBSs are distributed according to children points of TCP, we set $\sigma_v^2 = 1$, $\tilde{m} = 3$ per cluster, and hence, it makes $\lambda_{SBS} = 3$ per km^2. In order to set the intensity of the BSs in the network we define $\lambda_{BS} = \lambda_p(\tilde{m} + 1)$.

We subdivide this section into two parts as follows. In the first part, we validate our derived analytical expressions with numerical simulation. In the second part, we study the effect of varying different parameters of interest.

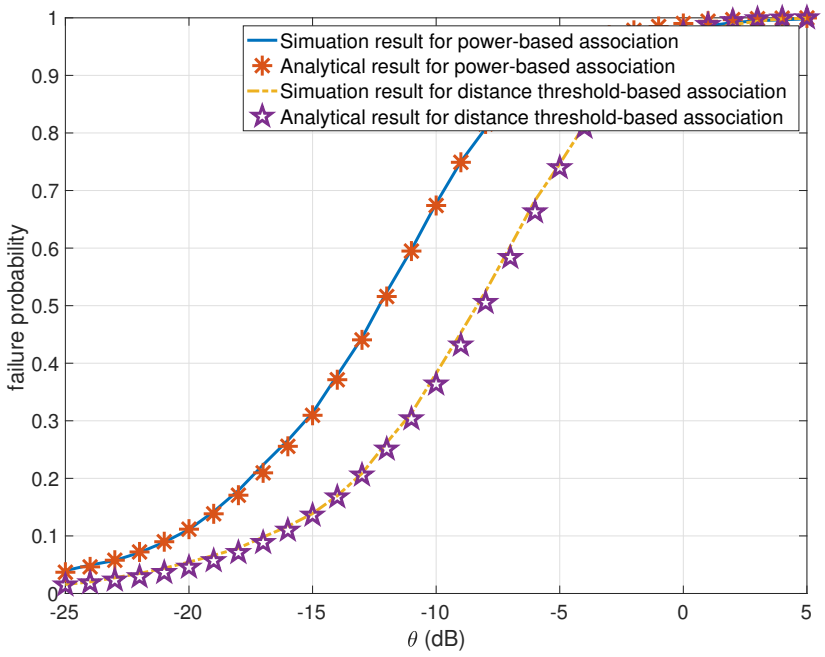

Figure 4.4: Failure probability versus SINR threshold θ for two-tier UL network where SBSs and MBSs are distributed according to PPP.

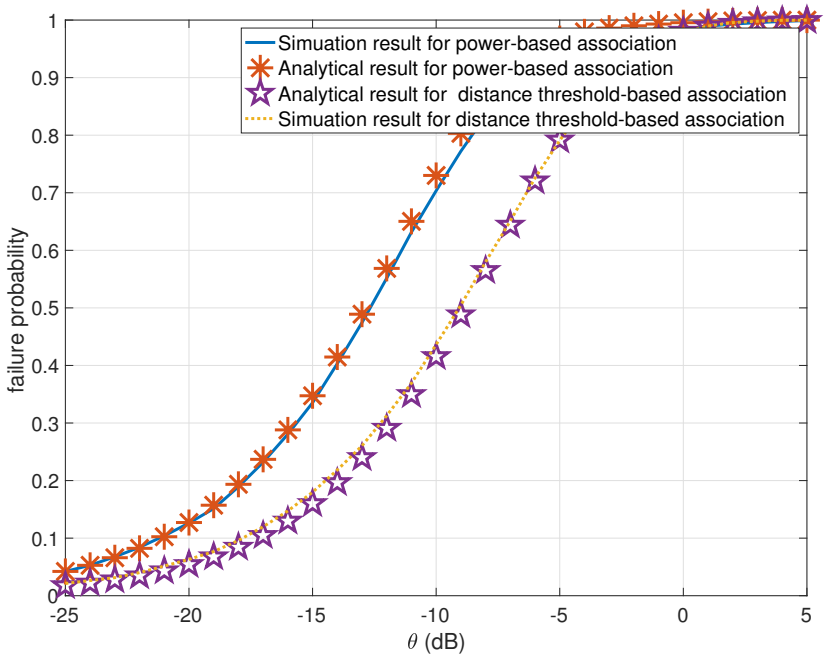

Figure 4.5: Failure probability versus SINR threshold θ for two-tier UL network where SBSs and MBSs are distributed according to parent and children points of MCP.

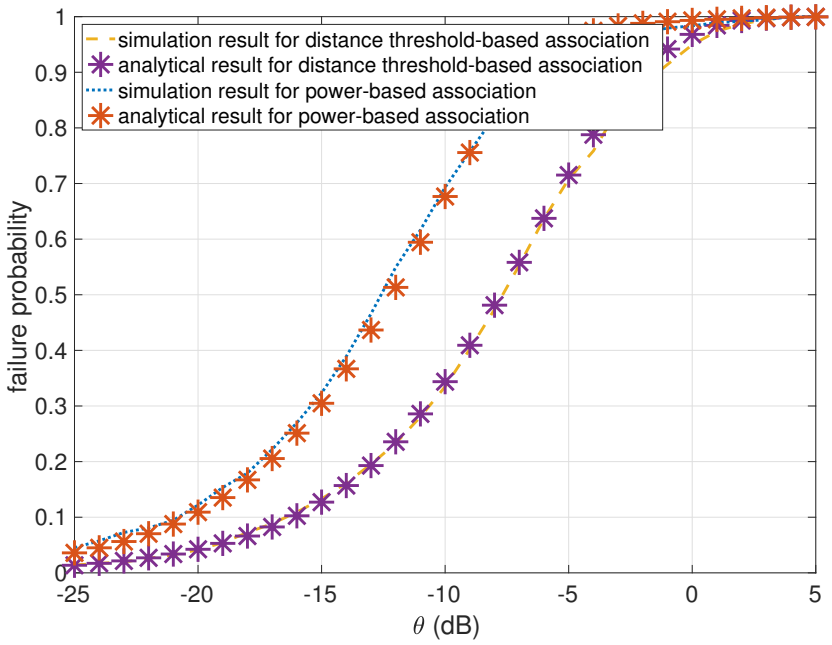

Figure 4.6: Failure probability versus SINR threshold θ for two-tier UL network where SBSs and MBSs are distributed according to parent and children points of TCP.

4.3.1 Validation of Analytical Results

4.3.1.1 Failure probability

In Figs. 4.4, 4.5, and 4.6 we plot the failure probability versus target SINR threshold for distance threshold-based association and power-based association for all three system models considered. Corresponding simulation results are also plotted in these figures. We use Monte Carlo method for obtaining the simulation results. From these figures, it is obvious that the analytical results are in agreement with the simulation results. We also observe that for all cases, the failure probability increases as the SINR threshold increases, as expected. An interesting observation is, for power-based association the failure probability if higher than distance threshold-based association. The reason is, while following the power-based association scheme, the device transmits the connection request with the lowest amount of power. The lowest amount of power leads to lower SINR, which causes the high failure probability. However, the difference in connection failure probability, between the two schemes, depends on the cluster size, distance threshold and the power control thresholds.

4.3.2 Effect of Varying Network Parameters:

In this section, we study the effect of varying the different network parameters on failure probability for each time slot. In particular, for the network model where BSs are distributed according to MCP, we vary cluster radius and device density on association probability, connection failure probability and average waiting time.

4.3.2.1 Effect of cluster size of on the association probability

Fig. 4.7 shows association probability of SBSs for different radius of Matérn cluster with distance threshold-based association scheme. For higher radius of Matérn cluster, the association probability of SBSs is also higher with distance threshold-based association scheme. When the radius of the cluster increases, more SBSs are distributed within a given area. Therefore,

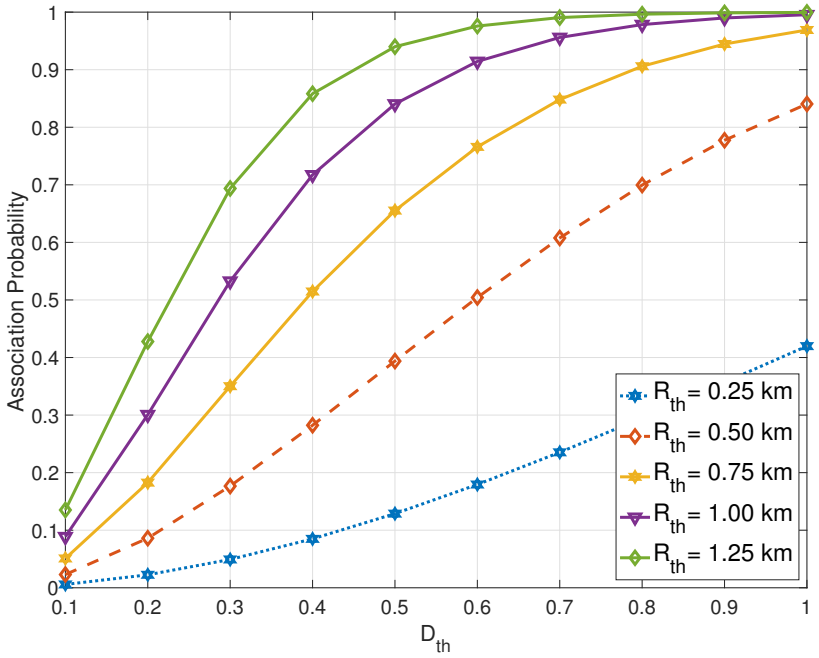

Figure 4.7: Association probability to small-tier BS for different radius of Matérn Cluster with distance threshold based association for $D_{\text{th}} = 0.8$ km.

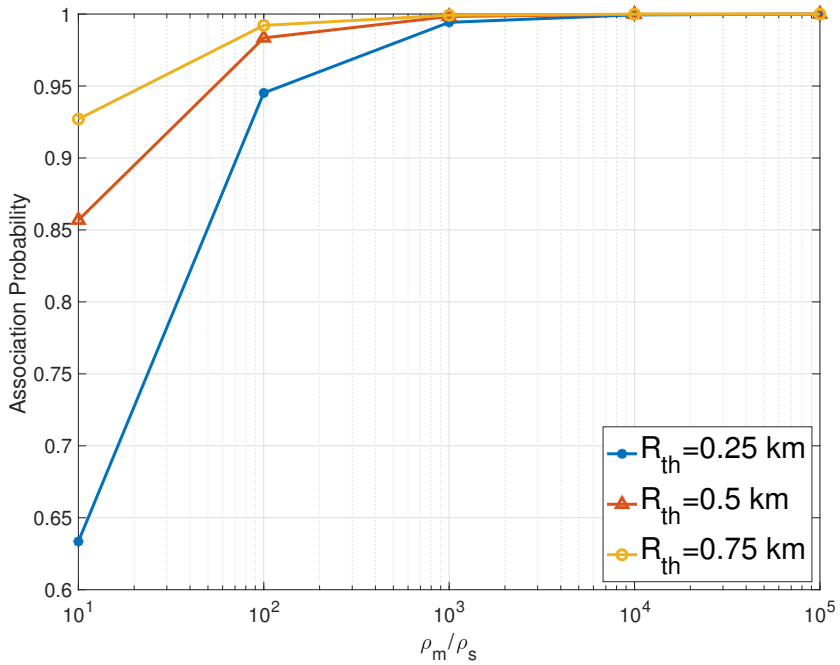

Figure 4.8: Association probability to small-tier BS for different radius of Matérn Cluster with power based association for different ratios of $\frac{\rho_m}{\rho_s}$ where $\rho_m = -90$ dBm.

the probability of a SBS being closer to a device is increased.

In Fig. 4.8, we show the association probability of SBSs for different values of radius of cluster when the power-based association scheme is employed. To plot this figure, we vary the ratio of ρ_m and ρ_s from 10^1 to 10^5 where we fix $\rho_m = -90$ dBm. From Fig. 4.8, we observe that as the value of $\frac{\rho_m}{\rho_s}$ increases, the association probability corresponding to the small-tier increases. The reason is explained as follows. As the value of $\frac{\rho_m}{\rho_s}$ increases the received power threshold for small-tier is (proportionally) lower than the macro-tier. So, in order to connect with a SBS, a device has to transmit a lower amount of power compared to that of a MBS. As such, the association probability of small-tier increases. From this figure, it is also obvious that as the R_{th} increases, the association probability corresponding to small-tier increases. This is expected as the value of R_{th} increases, more SBSs are deployed in a given area.

4.3.2.2 Effect of cluster size on the failure probability:

In order to show the effect of radius of the cluster on the failure probability, in Figs. 4.9 and 4.10, we plot failure probability versus SINR threshold for distance threshold-based and power-based associations schemes, respectively. For distance threshold-based association scheme, failure probability, plotted in Fig. 4.9, clearly shows that the failure probability increases as the value of R_{th} increases. This is due to the reason that when the value of R_{th} increases, more SBS are deployed in a given area. As such a typical device has a higher probability to connect to a BS within a smaller area.

Interestingly, for power-based association scheme, the failure probability plotted in Fig. 4.10 shows crossovers in high SINR threshold (θ) region. In other words, in the higher target SINR region, with the increment of R_{th}, failure probability increases rather than decreasing. The reason can be explained as follows. With the increment of R_{th} the association probability to connect with SBSs increases. As the devices follow the full-inversion power-control law, while the device intends to connect with a SBS, it experiences a lower signal power and a higher interference power. For lower values of

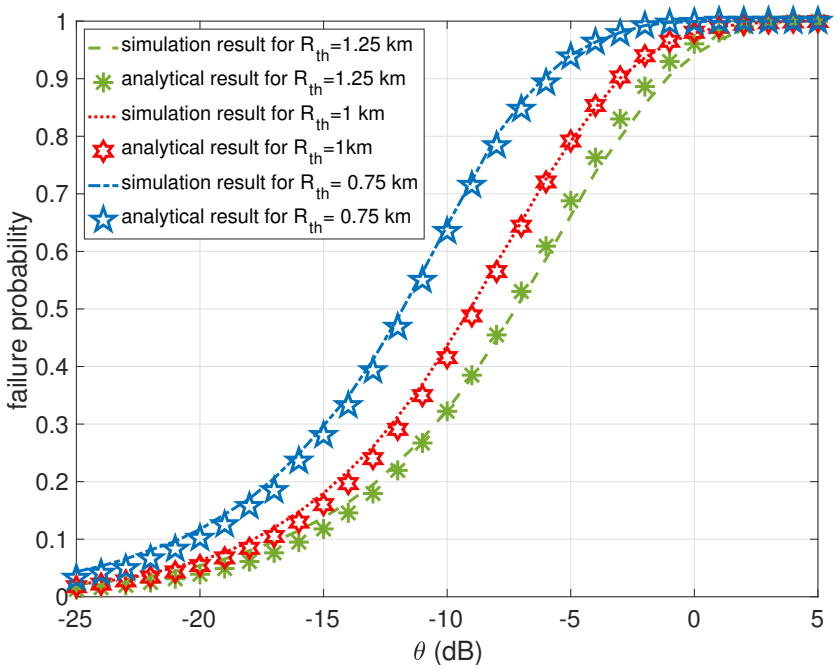

Figure 4.9: Failure probability versus θ for different cluster radius R_{th} with distance threshold-based association for $D_{\text{th}} = 0.8$ km.

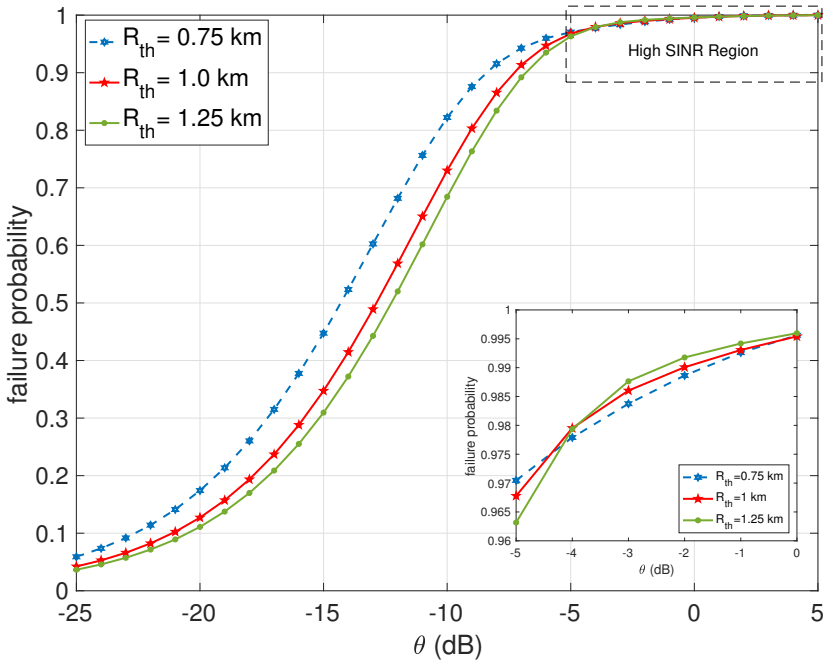

Figure 4.10: Failure probability versus θ with different cluster radius R_{th} in power-based association for $\rho_s = -100$ dBm and $\rho_m = -90$ dBm.

θ, it is easy to achieve such a threshold value for even higher values of R_{th}. Hence, the failure probability decreases with the increment of R_{th} up to a certain value of θ. After that value of θ, due to the higher interference power and the lower signal power, the devices tend to fail to achieve the higher SINR threshold when the value of R_{th} increases. Therefore, the target threshold increases with the increment of R_{th}, and failure probability increases instead of decreasing. In this region failure probability decreases with decrement of R_{th}. In distance threshold-based association scheme, we do not observe this trend because of the assumption of same received power threshold for all tiers.

The analysis provides an engineering insight that can assist to design networks as demonstrated via example applications. For example, the radius of cluster size, R_{th} should be higher to minimize the connection failure probability when the distance threshold-based association scheme is employed as shown in Fig. 4.9. On the other hand, when power-based association scheme is employed, the value of R_{th} should be chosen based on the target SINR, θ. For example, as shown in Fig. 4.10, for the given parameters, if the target SINR threshold is below -4 dB, then R_{th} should be higher to achieve a lower connection failure probability. However, if the SINR requirement is larger than -4 dB, we should choose a lower value of R_{th} to have a lower value of failure probability.

4.3.2.3 Effect of traffic per BS:

One of the main objectives of our performance derivation is to study how to ensure a certain failure probability for given SINR requirement and devices' intensity. As such network designer can set values of various design parameters.

In Figs. 4.11 and 4.12, we plot the failure probability for different ratio of the devices' and BSs' intensities. From these figures, one can estimate the required intensity of the deployed BSs, λ_{BS} for given values of θ, λ_u, and connection failure probability. For example, from Fig. 4.11, if we fix the SINR threshold $\theta = -5$ dB and we want to maintain the failure probability

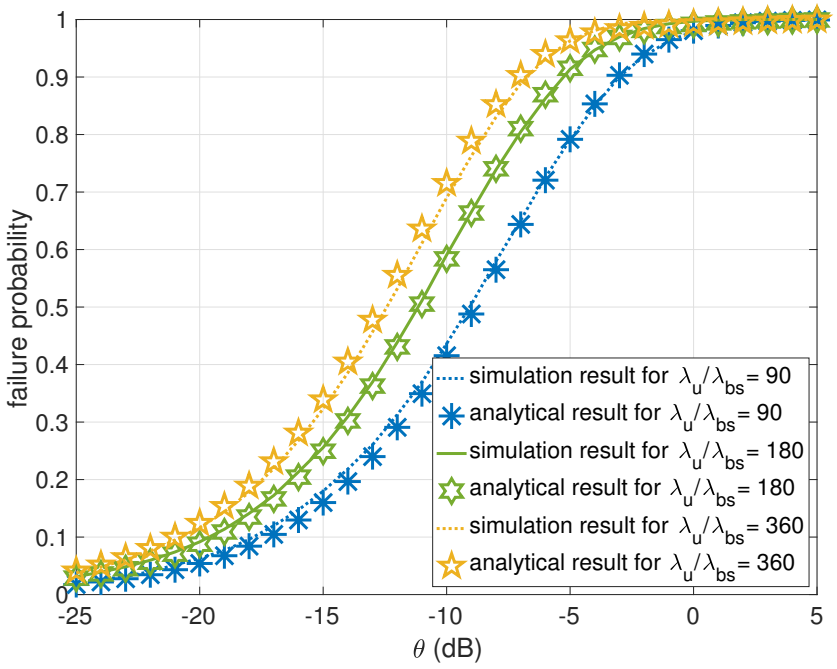

Figure 4.11: Failure probability versus θ for different $\frac{\lambda_u}{\lambda_{BS}}$ where $\lambda_u = 6n_Z, 12n_Z, 24n_Z$ per km^2, $n_Z = 60$ ZC sequences per BS, and $\lambda_{BS} = 4$ per km^2 under distance threshold-based association for $D_{\text{th}} = 0.8$ km.

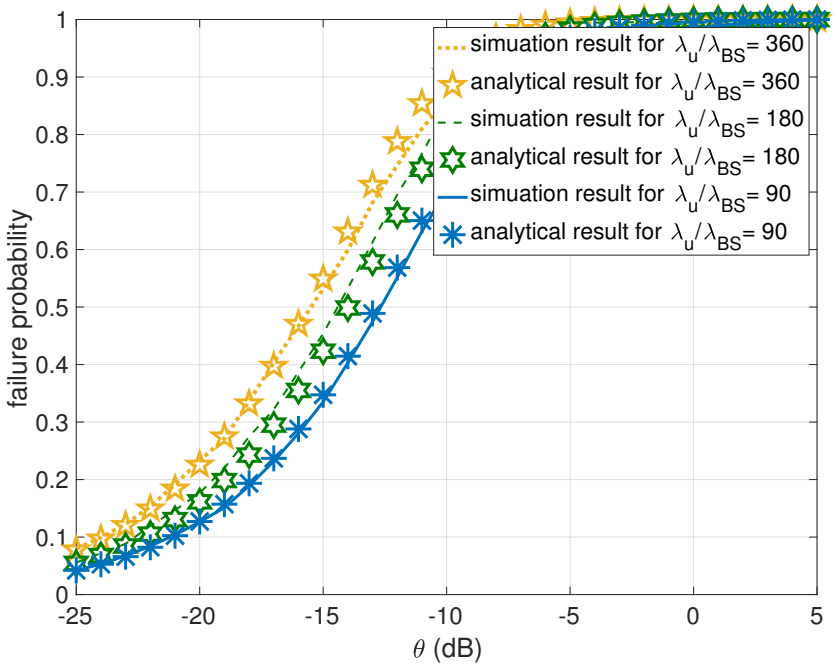

Figure 4.12: Failure probability versus θ for different $\frac{\lambda_u}{\lambda_{BS}}$ where $\lambda_u = 6n_Z, 12n_Z, 24n_Z$ per km^2, $n_Z = 60$ ZC sequences per BS, and $\lambda_{BS} = 4$ per km^2 under power-based association for $\rho_s = -100$ dBm, and $\rho_m = -90$ dBm.

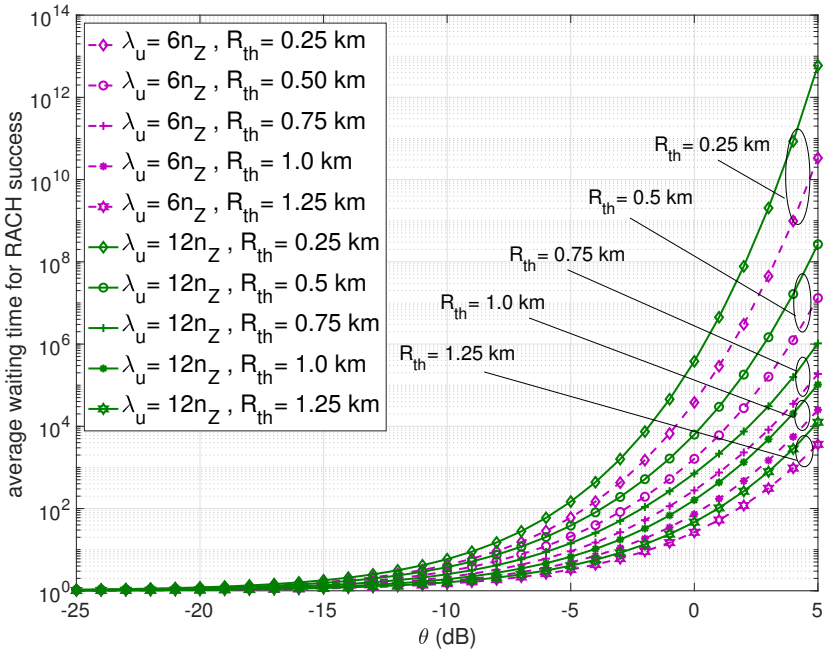

Figure 4.13: Average waiting time for RACH success, $\mathcal{D}$ for different cluster radius and device density.

to be less than 80% the intensity of the devices should be maximum 90 times of the intensity of BSs, where $n_Z = 60$ ZC sequences per BS. These figures also confirm the trend of saturation of the network with the increase of the devices' intensity.

4.3.2.4 Effect of cluster size and device density on average waiting time for RACH success:

In this section we analyze the average waiting time (in no. of time slots) for RACH success by varying the cluster size and the device density by plotting the average waiting time in Fig. 4.13. From this figure, we observe that with a smaller cluster size and a higher device density, delay for successful connection increases. Apart from this, from Fig. 4.13 it can be seen that for a smaller cluster size, the spread of average waiting time between device densities is higher than that of larger cluster size. This result enlightens the fact that with a larger cluster size the delay in successful connection can be decreased even with higher user density. Fig. 4.13 considers distance threshold-based association; however, the power-based association concludes with similar remark.

4.4 Summary

In this chapter, we have developed a generalized approach to calculate connection failure probability of IoT devices in the RACH phase of UL transmission in a multi-tier network. The proposed approach was used to study the failure probability under two different association schemes. Using our derived failure probability, we have investigated the effect of various parameters on connection failure probability. As demonstrated via example applications, the presented analysis can assist network designers to tune various design parameters in multi-tier network in order to meet certain connection probability.

Chapter 5

Conclusion and Future Direction

In this chapter, we summarize the contributions of this thesis, and propose some future works that have ensued from my research works.

5.1 Conclusion

Stochastic geometry, nowadays, has been popular to derive the performance metrics for networks with massive number of devices. PPP has recently been used for random network modeling due to its well-defined closed form expressions. If the BSs are PPP distributed, most recent literatures have considered Voronoi tessellations' cell area distribution to calculate the coverage area of each BS. However, the Voronoi cell area distribution is not a good approximation when the BSs are distributed according to PCP. In this work, we have developed a generalized approach to calculate connection failure probability of IoT devices in the RACH phase of UL transmission for IoT enabled cellular network.

In particular, we have derived association probability for different distributions of BSs. Using our approach, the performance metric is calculated for different BSs' distribution in single-tier and multi-tier topology. In Chapter 3, we have developed a novel approach for calculating failure probability of each time slot for RACH scheme in single-tier network. In Chapter 4, we extended our approach for RACH phase for different association schemes in multi-tier network. Presented numerical results showed the accuracy and adaptability for our mathematical model.

We have also shown that even for PPP, our approach for calculating fail-

ure probability is more accurate than the method using Voronoi tessellation's cell area distribution. Moreover, for a particular distribution in multi-tier network, when power-based association scheme is applied, some interesting behaviour of the network is observed in high SINR region with varying cluster sizes. The proposed approach, in this thesis, is novel, generalized, and more accurate than the existing framework.

5.2 Future Works

In what follows, we have mentioned three research works that can be pursued in future.

- In this work, we consider Rayleigh fading channel model because of its analytical tractability. Using Rayleigh fading it is possible to derive concise equation for Laplace transform of interference. One potential extension is to assume other fading models, e.g., Nakagami fading. We conjecture that other fading models may not lead to concise equation for Laplace transform of interference. As such, an approximation of Laplace transform or different options can be explored.

- While considering RACH access phase, we consider the failed devices will resend the RACH access request with same received power threshold at next time slot. This medium access control (MAC) transmission scheme, namely baseline scheme, can be replaced by other MAC transmission schemes, e.g., power ramping scheme.

- In this work, we consider the devices are distributed according to PPP. However, in real world devices can be dense at some places. To portray those cases PCP can be considered for devices' distribution and necessary derivations can be carried out.

Bibliography

[1] R. Khan, S. Khan, R. Zaheer, and S. Khan, "Future internet: The internet of things architecture, possible applications and key challenges," in *Proc. of International Conference on Frontiers of Information Technology (FIT)*, Islamabad, Pakistan, Dec. 2012. → pages 1

[2] J. M. Khurpade, D. Rao, and P. D. Sanghavi, "A survey on IoT and 5G network," in *Proc. of International Conference on Smart City and Emerging Technology*, Mumbai, India, Jan. 2018. → pages 1

[3] W. Ejaz, A. Anpalagan, M. A. Imran, M. Jo, M. Naeem, S. B. Qaisar, and E. Wang, "Internet of Things (IoT) in 5G wireless communications," *IEEE Access*, vol. 4, pp. 10310-10314, 2016. → pages 1

[4] B. A. Shargabi, and O. Sabri, "Internet of Things: An exploration study of opportunities and challenges," in *Proc. of International Conference on Engineering & MIS (ICEMIS),* Monastir, Tunisia, May 2017. → pages 1

[5] M. R. Palattella, M. Dohler, A. Grieco, G. Rizzo, J. Torsner, T. Engel, and L. Ladid, "Internet of things in the 5G era: Enablers, architecture, and business models," *IEEE Journal on Selected Areas in Communications*, vol. 34, no. 3, pp. 510-527, Mar. 2016. → pages 1

[6] A. Al-Fuqaha, M. Guizani, M. Mohammadi, M. Aledhari, and M. Ayyash, "Internet of Things: A survey on enabling technologies, protocols, and applications," *IEEE Communications Surveys & Tutorials*, vol. 17, no. 4, pp. 2347-2376, Jun. 2015. → pages 1

[7] D. Miorandi, S. Sicari, F. D. Pellegrini, and I. Chlamtac, "Internet of things: Vision, applications and research challenges," *Elsevier Ad Hoc Networks*, vol. 10, no. 7, pp. 1497-1516, 2012. → pages 1

[8] S. Mendhurwar and R. Mishra, "Emerging synergies between Internet of Things and social technologies," *Journal of Global Information Technology Management*, vol. 21, no. 2, pp. 75-80, Apr. 2018. → pages 1

[9] M. Sreeram and M. Sreeja, "A novel architecture for IoT and smart community," in *Proc. of International Conference on IoT in Social, Mobile, Analytics and Cloud (I-SMAC)*, Palladam, India, Feb. 2017. → pages 1

[10] IDC, "Internet of Things (IoT) 2013 to 2020 market analysis: Billions of things, trillions of dollars", Market Anal. Tech. Rep. 248451, 2013. → pages 1

[11] C. Drubin, "The internet of things will drive wireless connected devices to. 40.9 billion in 2020," *Microwave Journal*, vol. 57(10), no. 51, Aug. 2014. → pages 1

[12] A. Bader, H. ElSawy, M. Gharbieh, M. S. Alouini, A. Adinoyi, and F. Alshaalan, "First mile challenges for large-scale IoT," *IEEE Communications Magazine*, vol. 55, no. 3, pp. 138-144, Mar. 2017. → pages 1, 6, 9, 33, 63

[13] D. Evans, *Cisco White Paper: The internet of things: How the next evolution of the internet is changing everything.* CA, USA, Apr. 2011. → pages 1, 2

[14] *White Paper: Cisco visual networking index: Global mobile data traffic forecast update, 2016-2021.* San Jose, CA, USA, Mar. 2017. → pages 1

[15] L. Atzori, A. Iera, and G. Morabito, "The internet of things: A survey," *Computer networks*, vol. 54, no. 15, pp. 2787-2805, May 2010. → pages 2

[16] S. S. I. Samuel, "A review of connectivity challenges in IoT-smart home," in *Proc. of MEC International Conference on Big Data and Smart City (ICBDSC)*, Muscat, Oman, Mar. 2016. → pages 2

[17] A. Scott, "The Future is Smart: 8 ways the Internet of Things will change the way we live and work," [Online]. Available:`https://www.theglobeandmail.com/report-on-business/rob-magazine/the-future-is-smart/article24586994/#transportation`. [Accessed: 24 Mar. 2019] → pages 2

[18] S. Andreev, O. Galinina, A. Pyattaev, M. Gerasimenko, T. Tirronen, J. Torsner, J. Sachs, M. Dohler, and Y. Koucheryavy, "Understanding the IoT connectivity landscape: A contemporary M2M radio technology roadmap," *IEEE Communications Magazine*, vol. 53, no. 9, pp. 32-40, Sep. 2015. → pages 2

[19] S. Pradeep, T. Kousalya, K. M. A. Suresh, J. Edwin, "IoT and its connectivity challenges in smart home," *International Research Journal of Engineering and Technology*, vol. 3, no. 12, pp. 1040-1043, Dec. 2016. → pages 4

[20] M. Frustaci, P. Pace, G. Aloi, and G. Fortino, "Evaluating critical security issues of the IoT world: Present and future challenges," *IEEE Internet of Things Journal*, vol. 5, no. 4, pp. 2483-2495, Aug. 2018. → pages 4

[21] L. Coetzee, J. Eksteen, "The Internet of Things-Promise for the Future? An Introduction," in *Proc. of IST-Africa*, Gaborone, Botswana, May 2011. → pages 4

[22] A. Haroon, W. Naeem, M. A. Shah, M. Kamran, Y. Asim, and Q, Javaid, "Constraints in the IoT: The world in 2020 and beyond," *International Journal of Advanced Computer Science and Applications*, vol. 7, no. 11, pp. 252-271, 2016. → pages 5

[23] "C-RAN the road towards green RAN," China Mobile Research Institute, Beijing, China, Tech. Rep., Oct. 2011. → pages 6

[24] M. Gharbieh, H. ElSawy, A. Bader, and M. S. Alouini, "Tractable stochastic geometry model for IoT access in LTE networks," in *Proc. of IEEE Global Communications Conference (GLOBECOM)*, Washington, DC, USA, Dec. 2016. → pages 6, 9, 11, 12, 21, 32, 33, 37, 50, 54, 56, 63

[25] M. Gharbieh, H. ElSawy, A. Bader, and M. S. Alouini, "Spatiotemporal stochastic modeling of IoT enabled cellular networks: Scalability and stability analysis," *IEEE Transactions on Communications*, vol. 65, no. 8, pp. 3585-3600, Aug. 2017. → pages 9, 11, 50, 54

[26] M. Gharbieh, H. ElSawy, A. Bader, and M. S. Alouini, "A spatiotemporal model for the LTE uplink: Spatially interacting tandem queues approach," in *Proc. of IEEE International Conference on Communications (ICC)*, Paris, France, Jul. 2017. → pages 6, 9

[27] H. ElSawy, E. Hossain, and M. Haenggi, "Stochastic geometry for modeling, analysis, and design of multi-tier and cognitive cellular wireless networks: A survey," *IEEE Communications Survey and Tutorials,* vol. 15, no. 3, pp. 996-1019, Jun. 2013. → pages 7, 23

[28] R. W. Heath, M. Kountouris, and T. Bai, "Modeling heterogeneous network interference using Poisson point processes," *IEEE Transactions on Signal Processing* vol. 61, no. 16, pp. 4114-4126, Aug. 2013. → pages 7

[29] H. S. Dhillon, R. K. Ganti, F. Baccelli, and J. G. Andrews, "Modeling and analysis of K-tier downlink heterogeneous cellular networks," *IEEE Journal on Selected Areas in Communication*, vol. 30, no. 3, pp. 550-560, Apr. 2012. → pages 7

[30] C. Lee, C. Shih, and Y. Chen, "Stochastic geometry based models for modeling cellular networks in urban areas," *Wireless Networks*, vol. 19, no. 6, pp.1063-1072, Aug. 2013. → pages 7

[31] H. Martin, J. Andrews, F. Baccelli, O. Dousse, and M. Franceschetti, "Stochastic geometry and random graphs for the analysis and design of

wireless networks," *IEEE Journal on Selected Areas in Communication*, vol. 27, no. 7, pp. 1029- 1046, Sep. 2009. → pages 7

[32] M. Haenggi, *Stochastic geometry for wireless networks*, Cambridge University Press, 2012. → pages 7, 18, 93, 98, 99

[33] S. Sesia, I. Toufik, and M. Baker, *LTE: the UMTS long term evolution.* Wiley Online Library, 2009. → pages 9

[34] N. Jiang, Y. Deng, X. Kang, and A. Nallanathan, "Random access analysis for massive IoT networks under a new spatio-temporal model: A stochastic geometry approach," *IEEE Transactions on Communications*, vol. 66, no. 11, pp. 5788-5803, Nov. 2018. → pages 9, 11, 33, 64

[35] M. Afshang and H. S. Dhillon, "Poisson cluster process based analysis of HetNets with correlated device and base station locations," *IEEE Transactions on Wireless Communications*, vol. 17, no. 4 ,pp. 2417-2431, Apr. 2018. → pages 11, 54

[36] Y. J. Chun, M. O. Hasna, and A. Ghrayeb, "Modeling heterogeneous cellular networks interference using Poisson cluster processes," *IEEE Journal on Selected Areas in Communications*, vol. 33, no. 10, pp. 2182-2195, Oct. 2015. → pages 11

[37] Z. Zeinalpour-Yazdi, and S. Jalali, "Outage analysis of uplink two-tier networks," *IEEE Transactions on Communications*, vol. 62, no. pp. 3351-3362, Jul. 2014. → pages 11

[38] D. Stoyan, W. Kendall, and J. Mecke, *Stochastic geometry and its applications,* 2nd edition. John Wiley and Sons, 1996. → pages 14

[39] R. W. Heath, M. Kountouris, and T. Bai, "Modeling heterogeneous network interference using Poisson point processes," *IEEE Transactions on Signal Processing*, vol. 61, no. 16, pp. 4114-4126, Aug. 2013. → pages 15

[40] C. Lee and M. Haenggi, "Interference and outage in Poisson cognitive networks," *IEEE Transactions on Wireless Communications*, vol. 11, no. 4, pp. 1392-1401, Apr. 2012. → pages 15, 16

[41] M. Haenggi and R. K. Ganti, "Interference in large wireless networks," in *Foundations and Trends in Networking.* NOW Publishers, 2008, vol. 3, no. 2, pp. 127-248. Available:`http://www.nd.edu/mhaenggi/pubs/now.pdf`. → pages 15, 23

[42] H. Tabassum, E. Hossain, and M. J. Hossain, "Modeling and analysis of uplink non-orthogonal multiple access in large-scale cellular networks using Poisson cluster processes," *IEEE Transactions on Communications*, vol. 65, no. 8, pp. 3555-3570, Aug. 2017. → pages 16

[43] M. Afshang, C. Saha, and H. S. Dhillon, "Nearest-neighbor and contact distance distributions for Matérn cluster process," *IEEE Communications Letters*, vol. 21, no. 12, pp. 2686-2689, Dec. 2017. → pages 16

[44] S. Joshi and R. K. Mallik, "Coverage and interference in D2D networks with poisson cluster process," *IEEE Communications Letters*, vol. 22, no. 5, pp. 1098-1101, May. 2018. → pages 18

[45] V. Suryaprakash, J. Møller, and G. Fettweis, "On the modeling and analysis of heterogeneous radio access networks using a Poisson cluster process," *IEEE Transactions on Wireless Communications*, vol. 14, no. 2, pp. 1035-1047, Feb. 2015. → pages 23

[46] H. ElSawy and E. Hossain, "On stochastic geometry modeling of cellular uplink transmission with truncated channel inversion power control," *IEEE Transactions on Wireless Communications*, vol. 13, no. 8, pp. 4454-4469, Aug. 2014. → pages 33, 64, 65

[47] M. A. Mathai, *An introduction to geometrical probability: Distributional aspects with applications*, New York, USA: Gordon and Breach, 1999. → pages 94

[48] M. Afshang, H. S. Dhillon, and P. H. J. Chong, "Modeling and performance analysis of clustered device-to-device networks," *IEEE Transactions on Wireless Communications*, vol. 15, no. 7, pp. 4957-4972, Jul. 2016. → pages 98

Appendices

Appendix A

Derivation of Void Probability with MCP

Let us consider a set of points are distributed in an area $A \subset \mathbb{R}^2$ ($0 < |A| < \infty$) according to a homogeneous PPP $\{x_1, x_2, x_3, \cdots\}$ (denoted as ψ_p) with density λ_p, and these points are the parent points (cluster centres) of the MCP. A set of SBSs are distributed according to PPP, denoted as $\psi_c = \{c_b; b = 1, 2, 3, \cdots\}$, with density λ_{ch} within a cluster centered at $x_{i'} \subset \psi_p$ around the parent point $x_{i'}$ in the circle of radius R_{th}. To derive the void probability, without loss of generality, we consider, a reference IoT device placed at the origin O. Let us denote $\mathbb{P}[\psi_c(D(O,r)) = 0]$ as the probability that there is no point from ψ_c in the disk $D(O,r)$ of radius r. By conditioning over the clusters, this probability expression is written as

$$\mathbb{P}[\psi_c(D(O,r)) = 0] = \mathbb{E}\left[\prod_{x\in\psi_p}\prod_{c\in\mathbb{N}_x} \mathbb{1}(x+c) \notin D(O,r)\right], \tag{A.1}$$

where x is a parent position of the cluster, ψ_p is the distribution of the clusters' parents, which is PPP distributed, $\mathbb{N}_x$ is the set of children of the parent x, and c is a children of that cluster. Using the Probability Generating Function (PGF) for PCP [32], eq. (A.1) can be simplified as

$$\mathbb{P}[\psi_c(D(O,r)) = 0] = \\ \exp\left\{-\lambda_p \int_{\mathbb{R}} \left(1 - e^{-\pi R_{\text{th}}^2 \lambda_{ch}}\right) \int_{D(x,R_{\text{th}})\cap D(O,r)} f_z(z|x)dzdx\right\}. \tag{A.2}$$

To find out $f_z(z|x)$ in eq. (A.2) we consider two cases shown in Fig. A.1.

1. *Case 1 (*$||x|| < R_{th}$*)* : In this case, the cluster centered at x includes the origin O. So, the children points, i.e., the BSs of this cluster, will reside either inside the disk $D(O, R_{\text{th}}-x)$ or in area $D(x, R_{\text{th}})\backslash D(O, R_{\text{th}}-x)$, where $C\backslash B = \{y \in C \mid y \notin B\}$. So, for this case $f_z(z|x)$ can be computed using [Theorem 2.3.6,[47]] as

$$f_z(z|x) = \begin{cases} A_1(z,x), & \text{if } 0 \leq z < R_{\text{th}} - x, \\ A_2(z,x), & \text{if } R_{\text{th}} - x \leq z \leq R_{\text{th}} + x, \end{cases} \tag{A.3}$$

where $A_1(z,x)$ and $A_2(z,x)$ are respectively defined as

$$A_1(z,x) = \frac{2z}{R_{\text{th}}^2}, \tag{A.4}$$

$$A_2(z,x) = \frac{2z}{\pi R_{\text{th}}^2} \cos^{-1}\left(\frac{z^2 + x^2 - R_{\text{th}}^2}{2zx}\right). \tag{A.5}$$

2. *Case 2 (*$||x|| > R_{th}$*)* : In this case, the cluster centered at x does not include the origin O. So, the children points, i.e., the BSs of this cluster, reside inside disk $D(x, R_{\text{th}})$. For this case, $x - R_{\text{th}} \leq z \leq R_{\text{th}} + x$, and $f_z(z|x)$ is equal to $A_2(z,x)$ defined in eq. (A.5).

In order to compute eq. (A.2), we need to find out the integral limits. For outer integral, in eq. (A.2) it is quite obvious to say that for Case 1, the integral limit spans from 0 to R_{th} whereas for Case 2, it spans from R_{th} to ∞. The inner integral, $\int_{D(x,R_{\text{th}})\cap D(O,r)} f_z(z|x)dz$, in eq. (A.2) can be simplified as

$$\int_{D(x,R_{\text{th}})\cap D(O,r)} f_z(z|x)dz = \begin{cases} \int_0^{\min(r,R_{\text{th}}-x)} A_1(z,x)dz, & \text{if } 0 \leq r < R_{\text{th}} - x \text{ and } ||x|| < R_{\text{th}} \\ \int_{\min(r,R_{\text{th}}-x)}^{\min(r,R_{\text{th}}+x)} A_2(z,x)dz, & \text{if } R_{\text{th}} - x \leq r \leq R_{\text{th}} + x \text{ and } ||x|| < R_{\text{th}} \\ \int_{\min(r,x-R_{\text{th}})}^{\min(r,x+R_{\text{th}})} A_2(z,x)dz, & \text{if } x - R_{\text{th}} \leq r \leq x + R_{\text{th}} \text{ and } ||x|| > R_{\text{th}}. \end{cases} \tag{A.6}$$

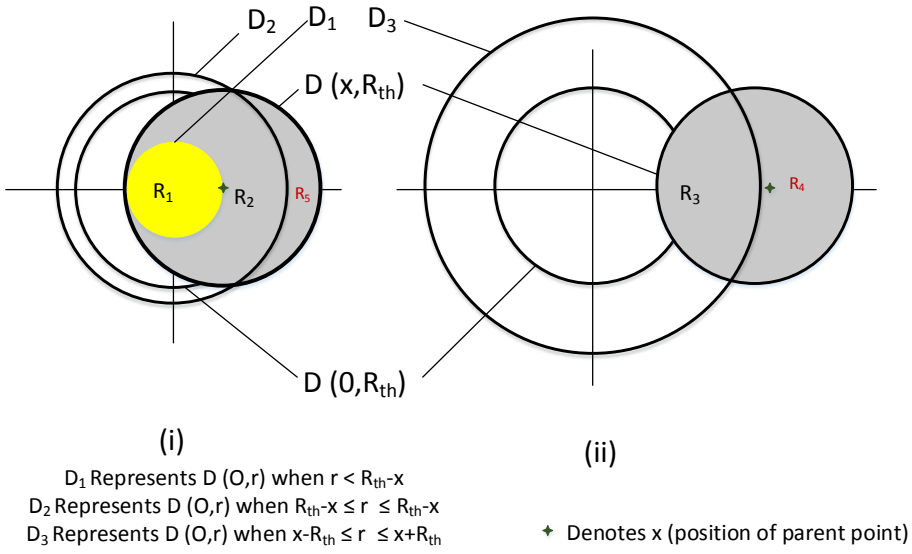

Figure A.1: Void probability scenarios: (i) Region R_1 and R_2 depict the scenarios for Case 1, and (ii) Region R_3 depicts the scenario for Case 2.

Using eqs. (A.4) , (A.5) and (A.6) in eq. (A.2) we obtain the void probability as

$$\mathbb{P}[\psi_c(D(O,r))=0]=\exp\Bigg(-2\pi\lambda_p\Bigg(\int_0^{R_{\rm th}}\Bigg[1-\exp\Bigg[-\lambda_{ch}\pi R_{\rm th}^2 \times\Bigg(\int_0^{\min(r,R_{\rm th}-x)}A_1(z,x)dz+\int_{\min(r,R_{\rm th}-x)}^{\min(r,R_{\rm th}+x)}A_2(z,x)dz\Bigg)\Bigg]\Bigg]xdx + \int_{R_{\rm th}}^{\infty}\Bigg[1-exp\Bigg(-\lambda_{ch}\pi R_{\rm th}^2\int_{\min(r,x-R_{\rm th})}^{\min(r,x+R_{\rm th})}A_2(z,x)dz\Bigg)\Bigg]xdx\Bigg)\Bigg). \quad (A.7)$$

After some manipulation in eq. (A.7) and changing the parameter from r to Z we obtain the void probability expression as

$$\mathbb{P}(\psi_c(D(O,Z))=0)= \exp\Bigg(-2\pi\lambda_p\Bigg(\int_0^{R_{\rm th}}\Bigg[1-\exp\Bigg[-\lambda_{ch}\pi R_{\rm th}^2\Bigg(\frac{(\min(Z,R_{\rm th}-x))^2}{R_{\rm th}^2} + I_1(x,Z)\Bigg)\Bigg]\Bigg]xdx+\int_{R_{\rm th}}^{\infty}\Bigg[1-\exp\Bigg(-\lambda_{ch}\pi R_{\rm th}^2 I_2(x,Z)\Bigg)\Bigg]xdx\Bigg)\Bigg), \quad (A.8)$$

where $I_1(x,Z)$ and $I_2(x,Z)$ are expressed as

$$I_1(x,Z)=C(\min(Z,R_{\rm th}+x),x)-C(\min(Z,R_{\rm th}-x),x), \quad (A.9)$$

$$I_2(x,Z)=C(\min(Z,x+R_{\rm th}),x)-C(\min(Z,x-R_{\rm th}),x), \quad (A.10)$$

where, $C(v,x)$ can be expressed as

$$C(v,x)=\frac{R_{\rm th}^2 v}{2\pi}\Bigg\{2v\cos^{-1}\left(\frac{v^2+x^2-R_{\rm th}^2}{2vx}\right) - x\sqrt{\frac{-R_{\rm th}^4+2R_{\rm th}^2(x^2+v^2)-(x^2-v^2)^2}{x^2v^2}}\Bigg\} - \frac{R_{\rm th}^4}{\pi}\tan^{-1}\left(\frac{-v^2+x^2+R_{\rm th}^2}{\sqrt{-R_{\rm th}^4+2R_{\rm th}^2(x^2+v^2)-(x^2-v^2)^2}}\right). \quad (A.11)$$

Eq. (A.8) can readily be used to calculate the association probability. However, we can obtain the lower boundary of void probability in eq. (A.8). Let us use two inequalities: $(1-\exp(-ax)) < ax$ and $\exp(-y_1) < \exp(-y_2)$ for $y_1 > y_2$. Now the lower bound of $\mathbb{P}(\psi_c(D(O,Z))=0)$ in eq. (A.8) can be written as

$$\mathbb{P}_L(\psi_c(D(O,Z))=0) = \exp\Bigg(-2\pi\lambda_p\Bigg(\int_0^{R_{\text{th}}}\Bigg[\Bigg[\lambda_{ch}\pi R_{\text{th}}^2\Bigg(\frac{(\min(Z,R_{\text{th}}-x))^2}{R_{\text{th}}^2}+I_1(x,Z)\Bigg)\Bigg]\Bigg]xdx + \int_{R_{\text{th}}}^{\infty}\Bigg[\Bigg(\lambda_{ch}\pi R_{\text{th}}^2 I_2(x,Z)\Bigg)\Bigg]xdx\Bigg)\Bigg). \tag{A.12}$$

This lower bound is useful for approximating the highest association probability of the tier with SBSs as well as the highest failure probability for a given cluster size. For very high value of R_{th}, we can show that $\mathbb{P}_L(\psi_c(D(O,Z))=0) \approx \mathbb{P}(\psi_c(D(O,Z))=0)$ is satisfied.

Then, we approximate eq. (A.8) in a closed form for a given limit of distance. We conclude the fact that for very small values Z, $I_1(x,Z)\to 0$ and $I_2(x,Z)\to 0$. Using this fact, eq. (A.8) can be approximated as

$$\widehat{\mathbb{P}}(\psi_c(D(O,Z))=0) = \exp[-\pi\lambda_p R_{\text{th}}^2\{1-\exp(-\pi\lambda_{ch}Z^2)\}]. \tag{A.13}$$

Note, this approximation is only true when $Z < \frac{R_{\text{th}}}{2}$.

Appendix B

Derivation of Void Probability with TCP

Let us consider that the parent points of TCP are distributed in an area $A \subset \mathbb{R}^2$ $(0 < |A| < \infty)$ according to a homogeneous PPP $\{x_1, x_2, x_3, \cdots\}$ (denoted as ψ_p) with density λ_p. Around these parent points, children points are distributed according to a symmetric normal distribution, denoted by ψ_c, with variance σ_v^2. Let us denote $\mathbb{N}_x$ is the set of offspring points for the cluster which is centred at $x \in \psi_p$. The number of children points per cluster, i.e., around per parent point, is Poisson distributed with mean $\tilde{m}$. To derive the void probability, without loss of generality, we consider, a reference IoT device placed at the origin O. Let us denote $\mathbb{P}[\psi_c(D(O,r)) = 0]$ as the probability that there is no point from ψ_c in the disk $D(O,r)$ of radius r. Let us denote $\mathbb{D}^x$ is the sequence of distance from a reference point to the offspring points of the cluster, i.e.; $\{p : p = ||x+y||, \forall y \in \mathbb{N}_x\}$. For any choice of the reference point, conditioning over the location of cluster parent, the conditional distribution of P is Rician with density function $f_P(p|q)$, where $q = ||x||$ [48]. $f_P(p|q)$ can be written as

$$f_P(p|q) = f_P\left(p|q, \sqrt{\sigma_v^2}\right) = \frac{x}{\sigma_v^2} \exp\left(\frac{-(p^2+q^2)}{2\sigma_v^2}\right) I_0\left(\frac{pq}{\sigma_v^2}\right), \qquad \text{(B.1)}$$

where $I_0(.)$ is modified Bessel function with order zero.

To find out $\mathbb{P}[\psi_c(D(O,r)) = 0]$, we use the properties of PGF. By definition [32], PGF of of a non-negative integer-valued random variable R is given by

$$G_R(s) = \mathbb{E}(s^R), \qquad \forall s \in [0,1]$$

$$
\begin{aligned}
&= \sum_{n=0}^{\infty} s^n \mathbb{P}[R = n] \\
&\overset{(a)}{=} \sum_{n=0}^{\infty} s^n p_n \\
&\overset{(b)}{=} p_0 s^0 + p_1 s^1 + p_2 s^2 + p_3 s^3 + \cdots ,
\end{aligned} \tag{B.2}
$$

where (a) follows from conversion of parameter $\mathbb{P}[R = n]$ to p_n, and (b) follows from Maclaurian series expansion. From eq. (B.2) we can derive the void probability as

$$p_0 = \mathbb{P}[R = 0] = G_R(0). \tag{B.3}$$

This property of PGF holds for both random variables and random process. Hence, deriving PGF for TCP leads to calculation of void probability of TCP. For a Poisson point process, ϕ_r with intensity λ_r in area $\mathbb{R}^2$, the PGF can be defined as [32]

$$G(s) = \mathbb{E}\left(\prod_{x \in \phi_r} s(x)\right) = \exp\left(-\lambda_r \int_{\mathbb{R}^2} (1 - s(x)) dx\right). \tag{B.4}$$

The PGF of of number of points, from the cluster residing in the disk $D(O, r)$, can be derived as

$$
\begin{aligned}
&G_R(s) = \mathbb{E}(s^R) \\
&= \mathbb{E}\left(s^{\sum_{x \in \psi_p} \sum_{y \in \mathbb{N}_x}}\right) \\
&= \mathbb{E}\left(\prod_{x \in \psi_p} \prod_{y \in \mathbb{N}_x} s^{\mathbb{1}\{||x+y|| < r\}}\right) \\
&\overset{(a)}{=} \mathbb{E}\left(\prod_{x \in \psi_p} \exp\left(-\tilde{m} \int_{\mathbb{R}^2} \left(1 - s^{\mathbb{1}\{||x+y|| < r\}}\right) f_Y(y) dy\right)\right) \\
&\overset{(b)}{=} \exp\left[-\lambda_p \int_{\mathbb{R}^2} \left\{1 - \left(\exp\left(-\tilde{m} \int_{\mathbb{R}^2} (1 - s^{\mathbb{1}\{||x+y|| < r\}}) f_Y(y) dy\right)\right)\right\} dx\right] \\
&\overset{(c)}{=} \exp\left[-\lambda_p \int_{\mathbb{R}^2} \left\{1 - \left(\exp\left(-\tilde{m} \int_{\mathbb{R}^2} (1 - s^{\mathbb{1}\{||z|| < r\}}) f_Y(z - x) dz\right)\right)\right\} dx\right]
\end{aligned}
$$

$$\stackrel{(d)}{=} \exp\left[-2\pi\lambda_p \int_0^\infty \left\{1 - \left(\exp\left(-\tilde{m}\int_0^r (1-s) f_P(p|q)dp\right)\right)\right\} qdq\right], \quad \text{(B.5)}$$

where (a) holds due to the reason that number of children points in each cluster is a PPP, (b) holds due to the fact that the parents points are distributed according to PPP, with $f_Y(y)$ defined in eq. (2.4), (c) follows from change in variable $z \leftarrow x + y$, and (d) follows from changing Cartesian to polar coordinates. In eq. (B.5), $f_P(p|q)$ is given in eq. (B.1). Hence the void probability $\mathbb{P}[\psi_c(D(O,r)) = 0]$ can be derived from eq. (B.5) as

$$\begin{aligned}
&\mathbb{P}[\psi_c(D(O,r)) = 0] = G_R(0) \\
&= \exp\left[-2\pi\lambda_p \int_0^\infty \left\{1 - \left(\exp\left(-\tilde{m}\int_0^r f_P(p|q)dp\right)\right)\right\} qdq\right] \\
&= \exp\left[-2\pi\lambda_p \int_0^\infty \left\{1 - \left(\exp\left(-\tilde{m}\left(1 - Q_1(\frac{q}{\sigma_v}, \frac{r}{\sigma_v})\right)\right)\right)\right\} qdq\right],
\end{aligned} \quad \text{(B.6)}$$

where $Q_1(a,b)$ is the first order *Marcum-Q-function*. Marcum-Q-function of order M is defined as $Q_M(a,b) = \exp -\frac{a^2+b^2}{2} \sum_{M-1}^{\infty} (\frac{a}{b})^{M-1} I_{M-1}(ab)$, where $I_{M-1}(ab)$ is modified Bessel function of order $M-1$.